Hot air recirculation enlarges efficient operating window of reversible solid oxide cell systems

A thermodynamic study of energy storage using ammonia

Amladi, Amogh; Venkataraman, Vikrant; Woudstra, Theo; Aravind, P. V.

DOI
10.1016/j.apenergy.2023.122276

Publication date
2024

Document Version
Final published version

Published in
Applied Energy

Citation (APA)
Amladi, A., Venkataraman, V., Woudstra, T., & Aravind, P. V. (2024). Hot air recirculation enlarges efficient operating window of reversible solid oxide cell systems: A thermodynamic study of energy storage using ammonia. *Applied Energy*, *355*, Article 122276. https://doi.org/10.1016/j.apenergy.2023.122276

Applied Energy 355 (2024) 122276

Contents lists available at ScienceDirect

Applied Energy

journal homepage: www.elsevier.com/locate/apenergy

Hot air recirculation enlarges efficient operating window of reversible solid oxide cell systems: A thermodynamic study of energy storage using ammonia

Amogh Amladi [a,b,*], Vikrant Venkataraman [a,c], Theo Woudstra [a,b], P.V. Aravind [a,b]

[a] Department of Process and Energy, Faculty of Mechanical, Maritime and Materials Engineering, Delft University of Technology, Leeghwaterstraat 39, 2628CB Delft, The Netherlands
[b] Energy Conversion Group, Energy and Sustainability Research Institute Groningen, Faculty of Science and Engineering, University of Groningen, Nijenborgh 6, 9747AG Groningen, The Netherlands
[c] Instrumentation and Test Systems, Conditioning Systems Hydraulics, AVL List GmbH, Hans List Platz 1, 8020 Graz, Austria

GRAPHICAL ABSTRACT

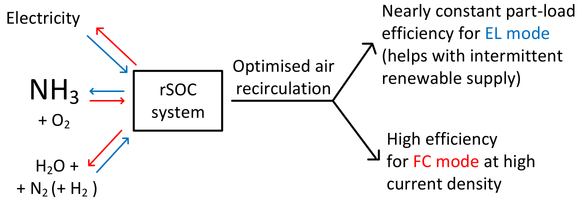

ARTICLE INFO

Keywords:
Reversible solid oxide cell
Exergy
Air recirculation
Ammonia
Energy storage
Fuel cell

ABSTRACT

Energy storage is vital for the energy transition, enabling reliable power grids based on intermittent renewables. Reversible solid oxide cell (rSOC) technology is promising for seasonal energy storage. The novel finding from this work is that optimised air recirculation for rSOC in endothermic electrolyser mode leads to efficiency being nearly independent of current density. Thereby the operating region of highest efficiency is expanded from the thermoneutral point to the entire endothermic region, leading to highly efficient part-load operation. Air recirculation increases fuel cell mode efficiency too, particularly at higher loads. This widens the efficient operating window in both modes. These findings emerge from a thermodynamic study of an rSOC-based energy storage system with ammonia as fuel. A process design is developed and optimised for efficiency, supported with detailed exergy analysis. First, ammonia synthesis subsystem integrated with the rSOC system in electrolyser mode is optimised. Second, rSOC outlet air recirculation is optimised for high system efficiency. Finally, rSOC operating points are optimised for highest round-trip efficiency. We find the least exergy destruction for the ammonia synthesis subsystem at 170 bar synthesis pressure and 30 °C condensation temperature (without needing refrigeration). The overall system achieves round-trip efficiencies up to 60.3%.

1. Introduction

The global renewable power generation capacity is expected to increase by around 1200 GW between 2019 and 2024 [1]. However, due to a mismatch between the fluctuations of renewable power generation and demand, the curtailment of renewable power generation has increased many-fold in the past decade [2], and can be expected to increase even further due to increasing penetration of renewable power sources. To avoid under-utilisation of this growing renewable power generation capacity, development and deployment of efficient large-scale energy storage technologies is needed on an urgent basis. A reversible solid oxide cell (rSOC) is a high-temperature electrochemical device that can be used in two modes: as a fuel cell (FC) or as an

---

[*] Correspondence to: Energy Conversion Group, Energy and Sustainability Research Institute Groningen, Faculty of Science and Engineering, University of Groningen, Nijenborgh 6, 9747AG Groningen, The Netherlands.
E-mail address: amogh.amladi@gmail.com (A. Amladi).

https://doi.org/10.1016/j.apenergy.2023.122276
Received 28 July 2023; Received in revised form 13 October 2023; Accepted 4 November 2023

electrolyser (EL). There are many advantages of energy storage systems using rSOC technology compared to competing large-scale energy storage technologies. These include high efficiency, independent scaling of system power and energy capacity, flexibility in system sizing and choice of fuels (i.e. energy carriers), and possible integration with waste heat sources and with other industries (particularly chemical industries) [3]. A recent case study on Texas and Germany has also shown that rSOCs are already profitable at hydrogen prices prevalent in small and medium-scale markets. It has also found that rSOCs are cost-competitive with separate FC and EL systems in both locations, being able to out-compete separate systems in Texas already, and in Germany in the near future [4]. Various fuels for rSOC systems have been suggested in literature that may be interesting for energy storage and industrial integration [3]. These include hydrogen, ammonia, methane, methanol and syngas.

There are many studies in literature with system-level thermodynamic analyses of rSOC-based energy storage. These studies have looked at various fuels, such as hydrogen [5–11], hydrogen mixtures with carbonaceous gases (including syngas) [11–14], methane [11,15,16], methanol [11,17], and ammonia [11,18,19].

Ammonia has several advantages as a fuel or energy storage medium. Compared to methane, hydrogen, or syngas, it can be liquefied under mild conditions (∼10 bar at 25 °C, or ∼−33 °C at 1 atm [20]), and thus, can be stored or transported easily. The Haber–Bosch process for ammonia synthesis is mature. It has remained fundamentally unchanged since its inception, with major improvements only in the production and purification of the hydrogen-nitrogen synthesis mixture [21]. Ammonia synthesis is exothermic, which promotes its integration with steam electrolysis. Like methane, ammonia can be cracked by nickel within the rSOC in FC mode, absorbing some of the heat generated by the electrochemical reaction and assisting with thermal management of the stack [22]. Ammonia is also a clean fuel, with no NOx emission detected under 800 °C [23,24] and less than 0.5 ppm at 950 °C [25]. Therefore, NOx emission should not be a problem at the temperature of rSOC, which is limited to 800 °C in this paper. Ammonia has a large market, which can further buffer any excess or shortfall of renewable energy. However, there is very little literature on thermodynamics of energy storage systems using rSOC with ammonia as fuel.

Ganzhou Wang et al. [18] designed and optimised an energy storage system based on ammonia and rSOC, using 1-D numerical models. A maximum DC-to-DC round-trip efficiency (RTE) of 72% was achieved. One unique aspect of the work was that oxygen produced in EL mode and nitrogen produced in FC mode were stored as liquids. A coupled refrigeration cycle liquefied one gas while evaporating the other. The study included a techno-economic sensitivity analysis, but no thermodynamic sensitivity analysis or exergy analysis.

Ligang Wang et al. [11] carried out a thermodynamic optimisation and comparison of Power-to-X-to-Power systems, using fuels suggested by Venkataraman et al. [3]. They found that methane-based systems had the highest RTE (37%-54%), thanks to internal reforming in the rSOC in FC mode, and significant heat integration possibilities. Ammonia-based systems were found to have the lowest RTE (27%-43%), despite having the same benefits as methane. They stated the major drawback of ammonia-based systems to be the compression of hydrogen up to 200 bar, needed for ammonia synthesis.

Mukelabai et al. [19] also studied ammonia-based rSOC systems. Their novelty was that hydrogen unutilised by the rSOC in FC mode was immediately reconverted to ammonia, instead of being combusted or stored. Their system achieved 41% or 53% RTE, depending on whether excess ammonia was exported or reused.

1.1. Research gap and research goals

- An exergy analysis of ammonia-based rSOC systems is not present in literature. Energy analysis (or first law analysis) can sometimes lead to misleading ideas about which components have the most scope for efficiency improvement, because even ideal components often cannot attain 100% energy efficiency. In comparison, exergy analysis (or second law analysis) effectively compares a real system to an ideal system. It therefore provides a more useful picture of which components are most inefficient, and can indicate possible improvement pathways for the system. Thereby exergy analysis plays an important role in system analysis.
  Therefore, the present work features a detailed thermodynamic exergy analysis of an ammonia-based rSOC energy storage system. An rSOC process chain is designed in Aspen Plus, and a sensitivity analysis is carried out for various rSOC operating conditions. The effects of several operating parameters are studied in detail through the use of sensitivity analysis from an exergy perspective. An optimum operating point is chosen on the basis of this analysis. Finally, an exergy analysis at the optimum point highlights the major sources of losses and opportunities for further improvement of efficiency.
- Several studies on solid oxide cell (SOC) systems have tested the recirculation of exhaust from the air electrode of an SOC (hereafter simply called "air recirculation") in FC mode [26–31]. They find that the use of air recirculation improves system efficiency, mainly by reducing air blower power. It also reduces system size and cost by allowing smaller heat exchangers. Some studies on EL mode have also recirculated air electrode exhaust (i.e. either O_2-enriched air or pure oxygen), which enhances system efficiency [31,32] and helps integrate waste heat from external sources [33].
  However, we are not aware of any study in literature that attempts to find the optimal amount of air recirculation for highest efficiency. Therefore, the present work also aims to find and implement the optimal amount of air recirculation in both FC and EL modes.
- In EL mode, the typical recommendation is to operate at or near the thermoneutral point [34]. This prevents large temperature gradients in the cells [35], and leads to highest system efficiencies [36,37]. This also simplifies the design by easing thermal management, thus reducing the air handling components, and also any direct heating/cooling for the stack [34,37]. But in a future with intermittent renewable energy sources, it can be expected that electrolysers will need to operate at part load for significant duration. For operating in EL mode at part-load (i.e. at lower current density), there are several possible strategies:
  - **Maintain thermoneutral voltage with nearly zero airflow**: At lower load (i.e. lower current density) the voltage tends to reduce due to lower losses. But at lower temperature, the voltage tends to increase due to higher reversible voltage and higher cell resistance. Therefore, to maintain thermoneutral voltage at part load without increasing airflow, the cell temperature can be reduced with reducing load, such that the effects of current density and temperature balance each other. This strategy can ensure almost constant efficiency over the operating range due to weak dependence of thermoneutral voltage on temperature [35]. However, this hampers the dynamic behaviour of the system, since stack temperature cannot be changed quickly due to the risk of cell damage.
  - **Endothermic operation with constant stack inlet temperature, and no airflow**: This reduces the stack outlet temperature and increases the temperature gradients across the cells. In order to prevent excessive temperature gradients, there is a lower limit on part-load operation when operating in this manner (for example, ∼75% of thermoneutral load [38]).

  - **Endothermic operation with heated sweep airflow providing the required heat**: This can avoid excessive thermal gradients, both spatial and temporal. However, this reduces the system efficiency [38,39], possibly due to the compression, exhaust, and other losses associated with sweep airflow.
  - **Endothermic operation with electric heating plates providing the required heat directly to the stack**: Since the temperature is controlled by the heating plates, partial load as low as 10% can be feasible [40]. However, there are also disadvantages to this approach. On the one hand, heating plates placed outside each stack may not effectively transfer heat to all cells in larger stacks for future large scale systems. On the other hand, addition of heating plates within each stack might lead to very complicated designs.

  Therefore, the strategies for part-load operation in literature each have some disadvantages. But the study of air recirculation in this work has revealed another approach for part-load operation. This approach can contribute to addressing the disadvantages of the currently existing strategies. This discovery is also described in this paper.

- Lastly, many papers present the results of their optimisation without a detailed explanation of the trends behind those results. One goal of this paper is to explain why certain things happen from a thermodynamic point-of-view, which the authors believe is not clearly explained in many papers. Offering detailed explanations will help readers to verify the results and to take this work forward. Therefore the authors have attempted to explain each observed trend in detail in this work.

To address these goals, an rSOC system using ammonia is modelled in this work. The model is described in Section 2. In Section 3, the ammonia synthesis subsystem is independently optimised, with consideration for the possible heat integration with the rSOC system. In Section 4, the effect of air recirculation from the rSOC is analysed, and optimal recirculation ratios are found for each rSOC operating point. In Section 5, these optimised parameters are used in simulations of the full rSOC system to optimise rSOC operating parameters for high system round-trip efficiency. Lastly, an exergy analysis of the optimised system shows pathways for future improvement.

2. Description of the model

This study uses a zero-dimensional system model built in Aspen Plus. It is based on similar models developed at TU Delft [14,41], and allows pressurised rSOC operation. The system incorporates several subsystems, such as the rSOC stack, gas purification system, and Haber–Bosch ammonia synthesis loop, along with other balance of plant (BoP) components. There is no dedicated ammonia cracker, since ammonia is assumed to be cracked at the fuel electrodes of the rSOC. This assumption is based on several studies [23,25,42–45] showing that the nickel catalyst in the rSOC fuel electrode can quickly crack ammonia almost completely, especially above 700 °C. For each operating mode of the system, a different heat exchanger network has been designed.

2.1. System model for fuel cell mode

The system model in FC mode is depicted in Fig. 1(a). Ammonia, which is stored as a liquid under pressure, is first expanded down to stack pressure. It is evaporated using heat from the environment and then further heated to the stack inlet temperature. It is then passed to the fuel electrodes of the rSOC where it undergoes thermal cracking and electrochemical oxidation. The model used for the rSOC stack is adapted from the work of Hauck et al. [46]. Details of the rSOC model are given in Appendix A. The exhaust gases from the fuel electrodes (steam, nitrogen and unutilised hydrogen) are sent to the separation system, where the steam is condensed out. The gases are further dried using temperature-swing adsorption (TSA) to the purity required for ammonia synthesis (< 5 ppm H_2O [21]). The dried gases are compressed and stored in a pressurised tank, to be reused for ammonia synthesis during EL mode. The condensed water is stored at ambient conditions, to be reused for electrolysis.

In this system, air is used both for thermal management and providing oxygen for fuel oxidation. Therefore, the air inlet temperature is maintained below the stack temperature. The temperature difference is maintained at 100 K to avoid excessive thermal gradients. Fresh atmospheric air is compressed to stack pressure, heated to the stack inlet temperature, and sent to the air electrodes. Part of the exhaust from the air electrodes is recirculated to reduce the requirement of fresh air. The remaining exhaust is expanded in a turbine, cooled to recover its heat, and released to the atmosphere.

The heaters and coolers shown in Fig. 1(a) are only indicative. In the actual model, these are replaced by a heat integration network, which is depicted in Fig. 1(b). The air from the turbine outlet is at low temperature, and can only preheat the fresh compressed air to a small extent. Therefore, the fuel electrode exhaust is used to heat both the fuel and the fresh air to high temperatures (i.e near the stack inlet temperature). If the streams are unable to attain the desired temperatures using heat exchangers alone, the network also includes backup electric heaters, and backup coolers using cold utility.

2.2. System model for electrolyser mode

The system model for EL mode is depicted in Fig. 2(a). Water from the tank is pumped to stack pressure, evaporated, and superheated to the required stack inlet temperature. Then the steam is mixed with an appropriate amount of gas recirculated from the fuel electrode outlet, so as to produce a mixture with 10% hydrogen content. This is to ensure a reducing atmosphere at the fuel electrodes [47]. This steam–hydrogen mixture is then sent to the rSOC fuel electrodes. The rSOC stack model for EL mode is elaborated in Appendix A. The produced hydrogen is purified using a condenser and a membrane separator to the required purity level. The separated water returns to the tank, while the pure hydrogen is compressed to the inlet pressure of the ammonia synthesis loop. Here, it is mixed with the compressed gas mixture stored from the FC mode, resulting in a feed gas with stoichiometric hydrogen-nitrogen ratio (3:1). This feed gas is introduced to the ammonia synthesis loop. The subsystem model of the ammonia synthesis loop, which is a part of Fig. 2(a), is elaborated in Section 2.3. Pure liquid ammonia is produced from the loop and stored in a pressurised tank.

In EL mode too, thermal management of the rSOC is done by manipulating the air-side flow. The air-side BoP in EL mode is almost identical to the FC mode. Depending on whether the electrolysis is exothermic or endothermic, the inlet air temperature is maintained 100 K lower or higher than the stack temperature, respectively. In order to reach temperatures higher than the stack temperature, an additional electric heater is placed just before the air electrode inlet. Because this heats the air above the stack temperature, it is hereafter referred to as the “air superheater”.

Similar to FC mode, the indicative heaters and coolers in Fig. 2(a) are replaced by a heat integration network, presented in Fig. 2(b). Most of the network (HEX1-HEX7) is dedicated to steam generation for electrolysis, which is very energy-intensive due to the large latent heat of water. Various small heat streams are employed from the hydrogen compressor intercoolers, the ammonia synthesis intercoolers, and the air-side exhaust. These are arranged in increasing order of temperature (HEX2-HEX6). High-temperature superheating is carried out using the fuel-side exhaust (HEX7). The heat of the ammonia synthesis reactor outlet is also used to preheat the synthesis feed mixture (HEX8).

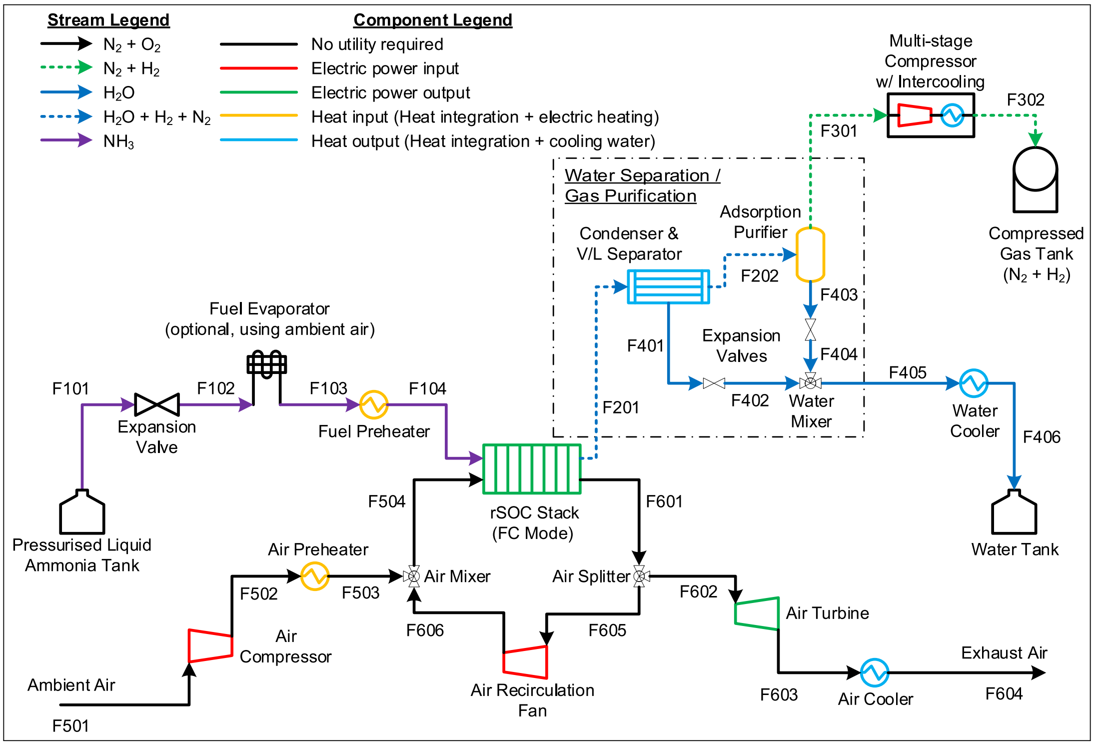

(a) System flowsheet

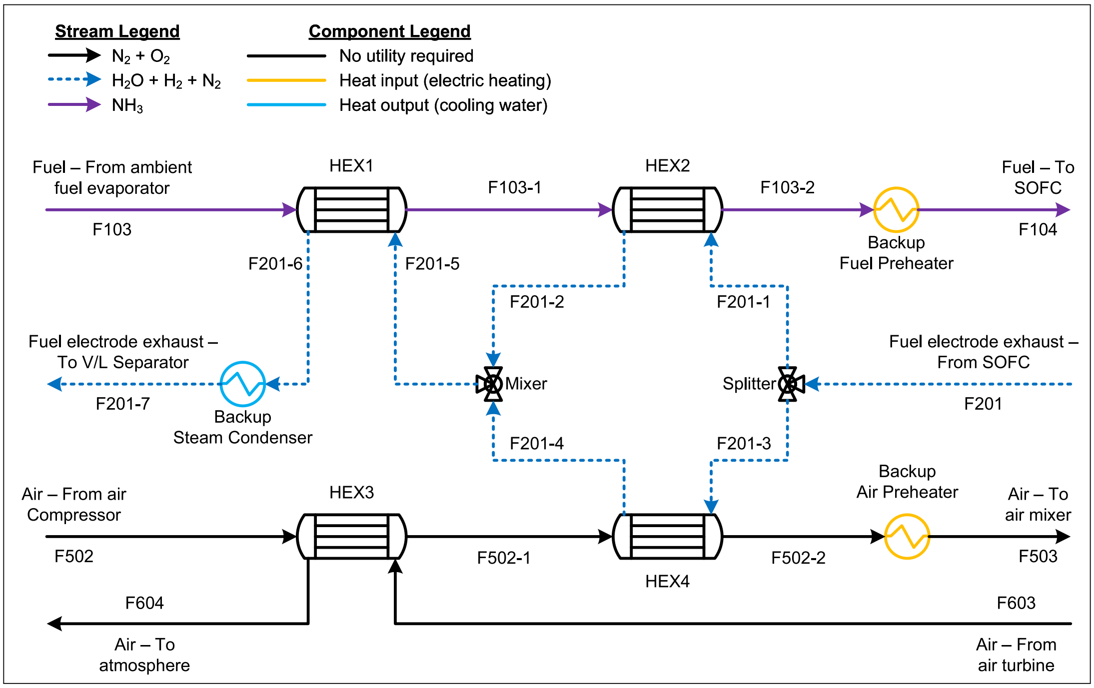

(b) Heat integration network

Fig. 1. System model flowsheet in fuel cell mode.

2.3. Ammonia synthesis subsystem (for electrolyser mode)

The ammonia synthesis subsystem is part of the EL mode system, shown in Fig. 2(a). Ammonia synthesis is carried out in a three-stage reactor using iron-based catalysts, with the stages modelled as adiabatic equilibrium reactors (RGIBBS in Aspen Plus). There is intercooling between the stages. This design is based on a study [48] that showed higher reactant conversion using indirect intercooling as opposed to quenching. The pressure drop in each stage is assumed to be 5 bar, which is within the range stated in literature [21]. The reactants are heated to 400 °C before the first reactor stage, and cooled down to the same temperature before each subsequent stage. The extent of the reaction in each stage is limited such that the maximum possible outlet temperature of each stage (i.e. before each intercooler) is 500 °C. The inlet and outlet temperature limits for the reactor are taken from literature [49]. Moreover, the extent of reaction in each stage is also

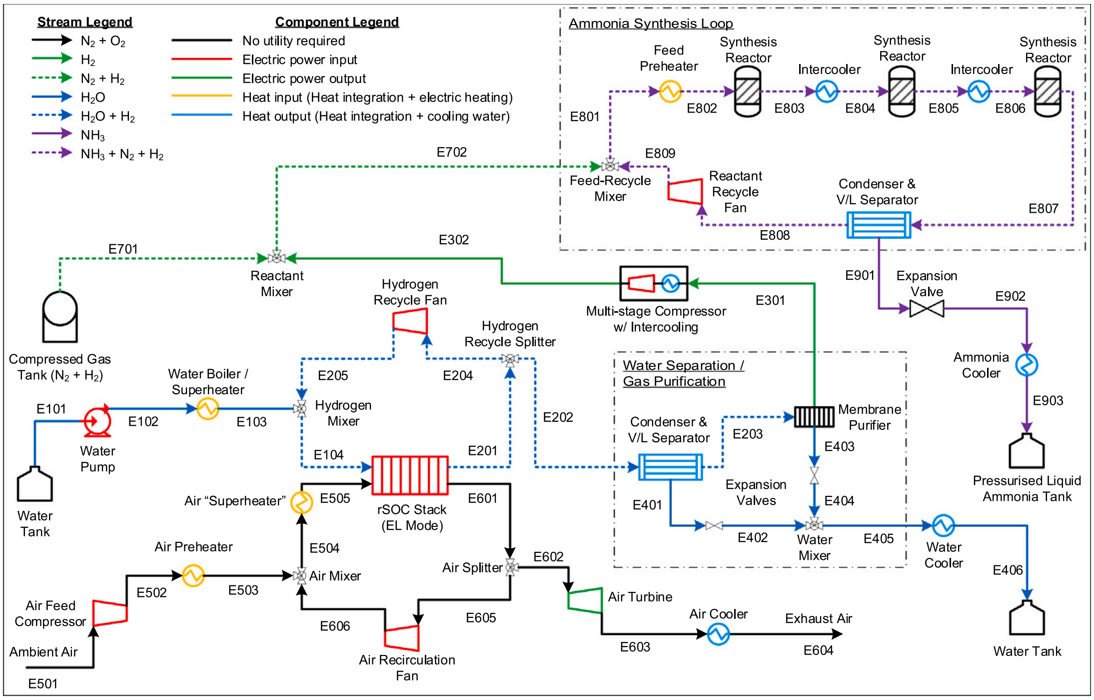

(a) System flowsheet

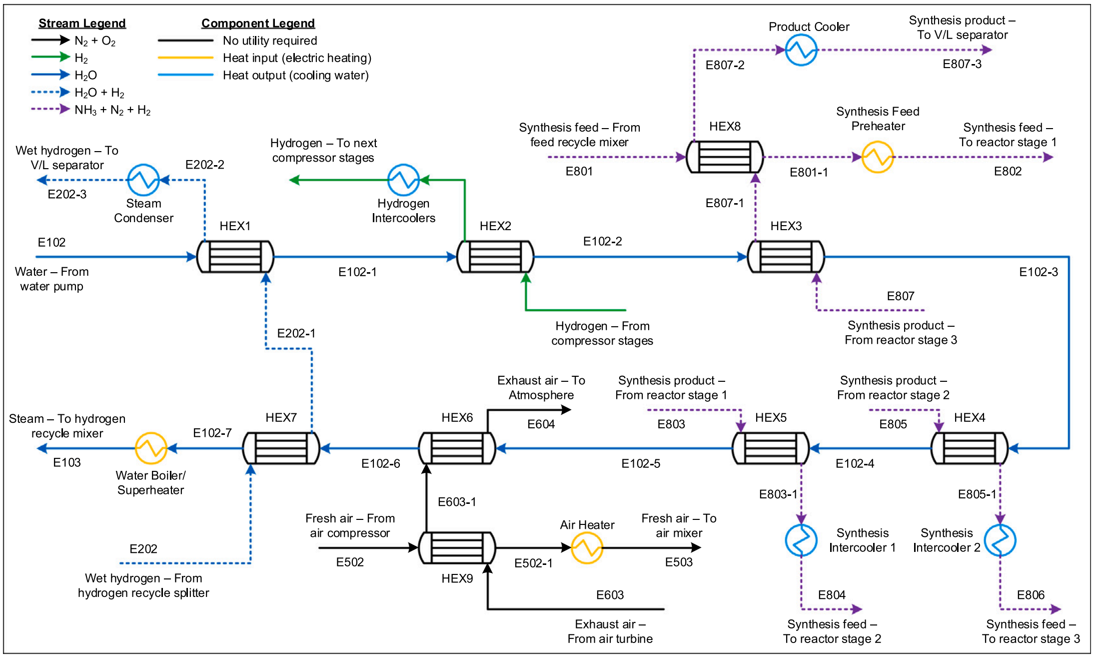

(b) Heat integration network

Fig. 2. System model flowsheet in electrolyser mode.

limited to a maximum of 80% approach to equilibrium[1] This approach to equilibrium is approximated with a 30 °C temperature approach[2] in the RGIBBS model. Both these limiting conditions, i.e. outlet temperature and approach to equilibrium, are based on the activity and temperature-tolerance of iron-based catalysts [50]. The extent of the reaction for each stage is chosen to be the lower one among the values predicted by these two limiting conditions. No purge is used since the feed gas coming into the loop is pure and in proper stoichiometric ratio. The produced ammonia is separated in a condenser, and the remaining feed gas (which is also in stoichiometric ratio) is recycled. The outlet pressure of the last reactor stage is 170 bar, while ammonia condensation is carried out at 30 °C, thus needing no refrigeration. These two values were chosen after optimising the synthesis loop for minimum exergy destruction, which is explained in detail in Section 3.

2.4. Balance of plant

Pressure-changing equipment is used in various places in the system. These are modelled differently based on their pressure ratio and flow rate, but the mechanical efficiency of all rotating equipment is assumed to be 95%. Hydrogen and nitrogen streams are compressed up to the ammonia synthesis pressure across the largest pressure ratios (between ∼17 and ∼1204, depending on operating mode and on stack pressure), but the flow rates of these streams are relatively small. Therefore, the compressors for these streams are modelled as multi-stage reciprocating compressors with intercooling. Since the variation in pressure ratio is so large, the number of stages is dynamically chosen (between 3 and 6) for each stack pressure, to keep the outlet temperature of each stage limited to 250 °C [51]. Each compressor stage is assigned a polytropic efficiency of 70% (between the U.S. Department of Energy's estimates for 2011 and 2015 [52]). The flow rate of air streams used for thermal management can be very large. The air compressor and turbine face a maximum pressure ratio of 10. Therefore they are modelled as single-stage axial machines, with an isentropic efficiency of 87.5% for compressors and 92.5% for turbines [53]. The compressors for the various recycle streams have very small pressure ratios (< 1.1) but relatively large flows. Therefore, these are assumed to be vane-axial fans with an isentropic efficiency of 85% [54]. The pumps for liquid ammonia and water are also assigned 85% efficiency. It must be noted that high temperature recirculation blowers have technical challenges, however a Technology Readiness Level (TRL) of 6 was already achieved in 2018 and further research has been ongoing [55]. Blowers for gases at 950 °C are commercially available [56], and have been used in SOC systems [57]. However, any heat loss caused by blade/housing cooling that might be required for these blowers has not been taken into consideration in this work.

In EL mode, hydrogen is the only gas to be separated from water vapour. Therefore, the purification system is assumed to be a hydrogen-selective membrane, with a pressure ratio of 10 across it [58]. In FC mode, both nitrogen and hydrogen have to be separated from water vapour. Therefore, a TSA system is used to adsorb and separate the water. In the study, this is simply modelled as an ideal separator followed by a heater which evaporates the separated water (to simulate the heat of desorption). This is a significant simplification of the energy consumption of TSA, but since the moisture content of the gases after condensation is quite small, this is considered an acceptable error.

In all systems, the heaters, coolers and heat exchangers are assigned a minimum temperature difference of 5 K. Heaters and coolers are assigned a pressure drop of 15 mbar [59]. The heat exchanger network, however, is not assigned any additional pressure drop.

Ambient conditions are assumed to be 25 °C and 1.013 25 bar. The water tank and the fresh air intake are assumed to be at ambient conditions. Ammonia is stored as a liquid at 11 bar and ambient temperature. The hydrogen-nitrogen gas mixture is stored at ambient temperature and 175.045 bar, based on the inlet pressure of the synthesis loop. The efficiencies of BoP components are assumed to independent of scale or load.

2.5. Exergy and efficiency calculations

Before defining the efficiency, some general assumptions for the system have to be specified, that make the formulation of efficiency definitions possible.

- No heat transfer is considered between the system and the environment (except via cooling water and air exhaust).
- All products (except oxygen) created in one mode are stored and completely utilised in the other mode. To ensure this, the system is operated in steady state, with the same current density, for equal duration in both operating modes.
- AC/DC conversion losses are not considered.
- The same stack temperature and pressure are chosen for both modes to avoid the complex dynamics of temperature and pressure changes in the high temperature system.

The exergy efficiency (second law efficiency) (η_{ex} [–]) for the entire system in each mode is defined in Eq. (1). The exergy difference between the air inlet and exhaust is considered as lost to the environment. Defining efficiency in this form is suitable for an energy storage system since the exergy traded with the grid (as electric power), and the exergy stored within the system (in chemicals) are separated on different sides of the fraction. Since exergy analysis is one of the main activities in this work, only exergy efficiency is calculated while energy efficiency is not stated.

$$\eta_{\mathrm{ex,FC}} = \frac{P_{\mathrm{net,FC,out}}}{\dot{E}x_{\mathrm{NH_3,in}} - \dot{E}x_{\mathrm{N_2/H_2,out}} - \dot{E}x_{\mathrm{H_2O,out}}} \tag{1a}$$

$$\eta_{\mathrm{ex,EL}} = \frac{\dot{E}x_{\mathrm{NH_3,out}} - \dot{E}x_{\mathrm{N_2/H_2,in}} - \dot{E}x_{\mathrm{H_2O,in}}}{P_{\mathrm{net,EL,in}}} \tag{1b}$$

The round-trip efficiency of an energy storage system (η_{RT} [–]) is defined as the ratio of the amount of energy that can be extracted from the system, to the energy that was originally put into the system. However, with all the assumptions mentioned above, this definition can be restated in terms of net electrical power for each mode, instead of electrical energy. This leads to Eq. (2), which is simply a product of the two parts of Eq. (1) when the above assumptions are considered.

$$\eta_{\mathrm{RT}} = \frac{P_{\mathrm{net,FC,out}}}{P_{\mathrm{net,EL,in}}} \tag{2}$$

The forms of exergy relevant to chemical processes are thermo-mechanical and chemical exergy. Aspen Plus can directly provide the thermo-mechanical exergy of any stream. Chemical exergy of any material stream is calculated as per procedures explained in literature [60]. Required values of standard chemical exergy are taken from literature [61]. The reference conditions for exergy analysis are the same as the assumed ambient conditions, i.e. 25 °C and 1.013 25 bar.

The exergy losses in this work are classified based on the type of process; such as electric heating, heat transfer, pressure changes (hereafter called "turbomachinery"), losses to the environment (via cooling utility and exhaust flows), etc. These losses often have different orders of magnitude. For the purpose of sensitivity analysis and optimisation, the changes in these values between different operating points matter more than the values themselves. In order to show all the values on one scale, the change in exergy losses is plotted instead of plotting the absolute loss values. The left-most value on each graph is the datum to measure change. Therefore, in the plots depicting exergy losses (such as the left axis in Fig. 5(b)), all lines start from a value of zero on the

---

[1] Approach to equilibrium is the ratio of the reaction quotient at the reactor outlet, and the equilibrium constant calculated at the outlet temperature.

[2] Temperature approach to equilibrium is the difference between the temperature at which the equilibrium constant is calculated, and the actual outlet temperature.

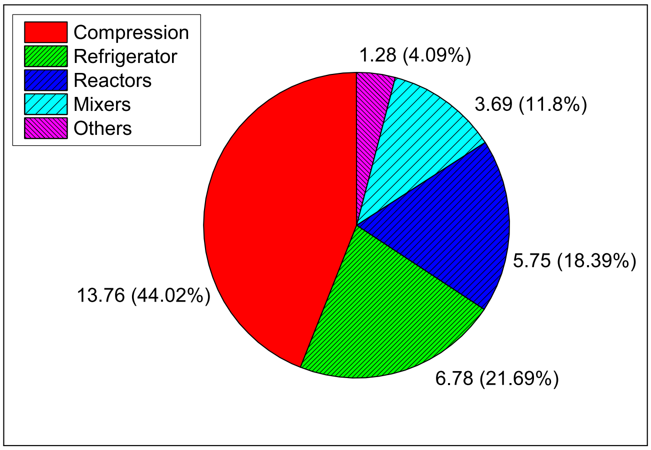

Fig. 3. Distribution of exergy destruction in ammonia synthesis - Base Case.

left. However, airflow rates, air recirculation ratios, efficiency values, etc. are plotted with absolute values on separate axes (such as the right axes in Fig. 5(b)).

The rSOC active area in the model is $30\,\mathrm{m}^2$ (i.e. 3000 cells of $10\,\mathrm{cm}\times 10\,\mathrm{cm}$). The system analysis is carried out with constant rSOC area and fuel/reactant utilisation. Therefore, all flow rates (except the airflow used for thermal management) are always directly proportional to the current density. The absolute magnitude of exergy losses can vary greatly simply based on flow rates (hence on current density), rather than changes in irreversibility. In order to make comparisons between different current densities easier, the exergy and mole flow rates in the following analyses are all normalised by the flow rate of ammonia at each current density (i.e. the units for exergy are $\mathrm{kJ/mol_{NH_3}}$ instead of kW or kJ, and units for flow rate are $\mathrm{mol/mol_{NH_3}}$ instead of $\mathrm{mol\,s^{-1}}$). It is important to note that the model does not consider the effects of scale. So the results would be the same at any stack area, and the assumed value ($30\,\mathrm{m}^2$) is arbitrary. This is another reason why the results are normalised as mentioned above.

3. Optimisation of ammonia synthesis subsystem

This section describes the optimisation of the ammonia synthesis loop, specifically the reactor outlet pressure and the ammonia condensation temperature. Wang et al. [11] found that feed gas compression to high synthesis pressure was a major cause of lower efficiency in ammonia rSOC systems. Therefore optimisation of the loop parameters, especially pressure, is needed to address these concerns. The condensation temperature is also optimised since it affects the feed recycle flow rate. The reaction temperature is not optimised in this case, since it is limited by catalyst properties (see Section 2.3). The subsystem model used for this optimisation is a slightly modified version of the model described in Section 2.3. The differences in the subsystem model are elaborated in Appendix D.1.

3.1. Methodology

The optimum operating point is chosen where exergy destruction in this subsystem are minimum. Instead of varying each variable separately while holding others constant, all variables are varied simultaneously, obtaining all possible combinations of variable values. This is done in an attempt to capture any effects that may not be visible when only one variable is varied at a time. Simulations are carried out on this model for all combinations of the following variable values:

Pressure at outlet of last reactor: 100 bar to 400 bar, at intervals of 10 bar

Condensing temperature: −35 °C to 40 °C, at intervals of 5 °C

The range of reaction pressures is chosen based on commonly used synthesis pressures (high pressures around 400 bar used in the past, and lower pressures of 100–200 bar used for newer plants with better catalysts). The range of condensation temperatures is chosen to start a little below the normal boiling point of ammonia (−33 °C) and end a little above ambient temperature.

To confirm that the optimisation is independent of rSOC pressure, it is repeated at five pressure values: 1.5 bar, 2.5 bar, 5 bar, 7.5 bar, and 10 bar. The rSOC pressure itself is not an optimised variable.

3.2. Base case

The base case for the ammonia synthesis system is a reactor outlet pressure of 200 bar and ammonia condensation temperature of −25 °C, which are within the typical range for modern plants [21]. The base case rSOC stack pressure is taken to be 5 bar.

The total exergy destruction for this operating point is found to be $31.25\,\mathrm{kJ/mol_{NH_3}}$, which is 7.5% of the total exergy input of $415.65\,\mathrm{kJ/mol_{NH_3}}$. The distribution of these losses is shown in Fig. 3. Almost half of the exergy destruction takes place during compression of feed gases. The refrigeration used for the ammonia condenser, and the synthesis reaction itself, are two other large causes of exergy destruction. The mixing of feed gases and the recycle stream also destroys some exergy due to the differing temperatures and compositions of the streams. The recycle fan, the heat exchanger and the expansion valve before the ammonia tank all make up a very small portion of the total losses.

$343.41\,\mathrm{kJ/mol_{NH_3}}$ is the exergy stored in ammonia. The coolers extract $68.03\,\mathrm{kJ/mol_{NH_3}}$, from which $27.04\,\mathrm{kJ/mol_{NH_3}}$ is used for feed gas preheating. The remaining $40.99\,\mathrm{kJ/mol_{NH_3}}$ (9.9% of total exergy input) is sent to the rSOC system for steam generation.

3.3. Optimum operating point for ammonia synthesis

The optimal operating point for ammonia synthesis in the context of the rSOC system was chosen as per the methodology set out in Section 3.1. For brevity, only a short summary of this optimisation is given here while a detailed analysis is given in Appendix D.

The optimal ammonia synthesis pressure depends strongly on the condensation temperature. At low condenser temperatures, the optimum synthesis pressure is between 220 bar and 270 bar. At high condenser temperatures, the optimum pressure is between 150 bar and 180 bar. This dependence on condenser temperature is mainly due to the recycle flow rate being very high when a combination of high condenser temperature and low synthesis pressure is implemented. More details can be found in Appendix D.2. In general, ammonia condenser temperatures above ambient were found to be the optimum. This is because condensation at these temperatures does not need refrigeration, significantly reducing exergy destruction. At low synthesis pressures, temperatures higher than 30 °C are not beneficial, once again due to very high recycle flow rates. More details can be found in Appendix D.3.

An overall comparison of all the tested operating points shows that minimum exergy destruction is achieved when the ammonia condenser temperature is 30 °C, and the pressure at the outlet of the last reactor is 170 bar. The condensing temperature being 30 °C eliminates the need for refrigeration and its exergy losses. Since the condensing temperature is high, the optimum reaction pressure is low as explained in Appendix D.2. Finally, since the reaction pressure is low, temperature above 30 °C is not preferred, leading to this optimal operating point.

For 5 bar stack pressure as an example, the minimised exergy destruction is $21.95\,\mathrm{kJ/mol_{NH_3}}$, compared to $31.25\,\mathrm{kJ/mol_{NH_3}}$ for the base case (6.1% and 7.5% of exergy input respectively). This is the combined result of all the trends explained in Appendix D. For other stack pressures, the optimised exergy destruction varies between $20.40\,\mathrm{kJ/mol_{NH_3}}$ and $25.20\,\mathrm{kJ/mol_{NH_3}}$ (both ~6% of exergy input).

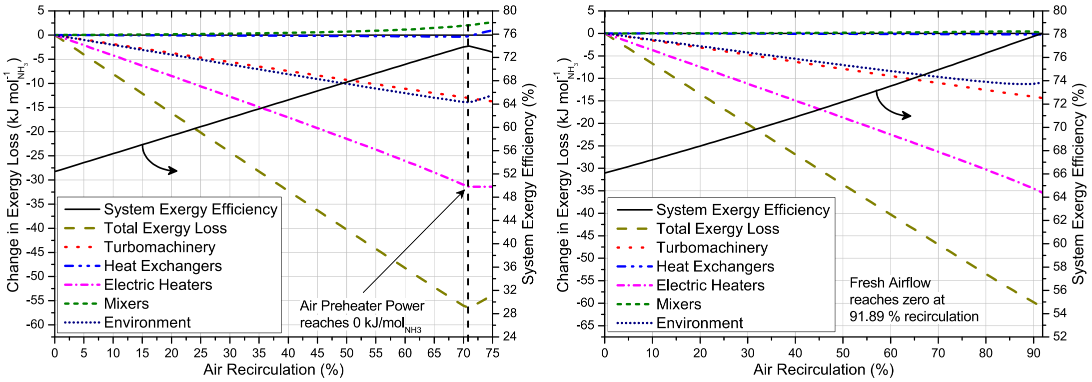

(a) Fuel cell mode. Stack operating point for this example: 7500 A m^{-2}, 800 °C, 7.5 bar.

(b) Endothermic electrolyser mode. Stack operating point for this example: 2500 A m^{-2}, 650 °C, 5 bar.

Fig. 4. Effect of air recirculation.

The optimum reaction pressure and condensing temperature are (almost) independent of stack pressure. The same operating point remains the optimum for all tested values of stack pressure, except one. Even in case of the single exception (i.e. 10 bar), it is only because a change in the number of hydrogen compressor stages causes a discontinuity (explained in Appendix D.2) which leads to 200 bar being optimum for that one case. Therefore, 170 bar and 30 °C is chosen as the operating point for the analysis of the overall rSOC system.

4. Effect of air recirculation

4.1. Methodology

The present work includes a sensitivity analysis based on various stack operating parameters, viz. current density, stack temperature, and stack pressure. The effect of fuel and steam utilisation, however, have not been addressed in this work, and are kept constant at 80%, which is within the typical range [62]. The following values of these three parameters are analysed, leading to 80 different operating points for each mode with different combinations of these parameters.

Current Density: 2500 A m^{-2}, 5000 A m^{-2}, 7500 A m^{-2}, 10 000 A m^{-2},

Stack Temperature: 650 °C, 700 °C, 750 °C, 800 °C

Stack Pressure: 1.5 bar, 2.5 bar, 5 bar, 7.5 bar, 10 bar

This section focuses on optimising air recirculation. Air recirculation ratio is defined as the ratio of the molar flow rate of recirculated air to the molar flow rate at air electrode outlet. For each of the 80 operating points mentioned above, an optimum value of air recirculation is found. This optimum air recirculation is used for further analysis of the other parametric effects on the entire system in Section 5.

4.2. Fuel cell mode results

The effect of air recirculation on system efficiency and on exergy losses in various operations in FC mode is depicted in Fig. 4(a). The total airflow through the stack is dictated by the heat generation in the stack, which is largely independent of air recirculation. When more air from the exhaust is recirculated, the amount of fresh air is reduced by the same amount in order to keep the airflow through the stack constant. Additionally, with greater recirculation of hot exhaust air, the preheating temperature of fresh air can also be reduced such that the mixed air input to the stack maintains a constant temperature, 100 K lower than the stack outlet.

Due to reduced fresh airflow as well as its lower preheating temperature, the electric preheating demand for fresh air significantly reduces with increased air recirculation. Correspondingly, the exergy destruction caused by this electric heating also reduces. This makes up the largest effect of air recirculation on exergy losses. Secondly, the flow rate of exhaust air released to the atmosphere is directly related to the amount of fresh air being drawn in. The temperature of the exhaust air is independent of air recirculation, since it is dictated by the temperature of the compressed fresh air (which is the flow with larger heat capacity in HEX3 in Fig. 1(b)). Thus, the exergy of the exhaust air is proportional to its flow rate, which reduces with increasing recirculation because of reduction in fresh air input. Therefore, as the air recirculation is increased, the exergy lost to the environment through the exhaust air decreases. Thirdly, the pressure and temperature of the airflows through the compressor and turbine are independent from air recirculation. Therefore, the exergy destruction in these components is directly proportional to the flow rate, and decreases as the recirculation is increased. Lastly, when a larger amount of hot exhaust air is mixed with the colder fresh air, the exergy destruction due to stream mixing increases. However, this change is overshadowed by the large exergy savings in the other operations. Therefore, the total system exergy losses decrease as the air recirculation is increased, and system exergy efficiency increases.

There is a sharp end to this trend, marked by the vertical line in Fig. 4(a). This occurs when the fresh airflow is reduced so much that heat integration alone is sufficient to preheat it, with no need for additional electric heating. When the electric heating requirement reaches zero in this way, no further reductions in exergy destruction of electric heating are possible. Moreover, if recirculation is increased beyond this point, exergy losses to the environment start increasing. This is not through the air exhaust, but rather through the cooling water used in the backup steam condenser seen in Fig. 1(b). Since electric heating is zero, any further decrease in air preheating demand due to increased recirculation means that the heat transferred through HEX4 has to be reduced. This implies an overall reduction in the heat extracted by the heat exchanger network from the fuel electrode exhaust. This additional heat is then released in the backup steam condenser, increasing the corresponding exergy loss. The reduced heat transfer in HEX4 also increases the temperature difference within HEX1, leading to larger exergy destruction there. Due to all these reasons, increasing air recirculation when the electric air preheating is already zero increases the total exergy losses and reduces the system efficiency.

Notably, air recirculation cannot be increased indefinitely in FC mode. Increasing air recirculation corresponds to a decrease in fresh airflow, as explained in the previous paragraphs. This reduces the oxygen concentration at the air electrode inlet and outlet. However, some oxygen is always needed to achieve the desired fuel utilisation in FC mode. Oxygen starvation may also cause cell damage. This imposes an upper limit on the amount of air recirculation. The research on the effects of oxygen starvation in rSOCs is sparse, but one study [63] found indications that oxygen concentration of ~4% can cause permanent damage to the cells. Therefore, we have used a minimum oxygen concentration of 4% at the air electrode outlet as the limit for air recirculation. Simple algebraic calculations show that oxygen concentration at the air electrode outlet is independent of the amount of air recirculation, depending only on oxygen consumption in the stack and fresh airflow from the atmosphere. Therefore, restricting the outlet oxygen concentration translates directly to limiting the fresh airflow. This depends on the oxygen consumption (i.e. on current density), but is independent of other parameters like air recirculation, stack temperature, or pressure. When normalised by the ammonia flow rate, the minimum fresh airflow limit is constant ($\sim 3.40\,\mathrm{mol/mol_{NH_3}}$).

There are some FC mode operating points where this minimum airflow limit is encountered before the electric air preheating can be reduced to zero. This leads to lower system efficiency compared to cases where the electric demand for air preheating does reach zero. The operating points where this oxygen starvation condition is encountered tend to be the points where rSOC stack efficiency is around its maximum (it is well known that highest FC stack efficiency occurs at high stack temperature, high stack pressure, and low current density). This is because when the stack is efficient, the excess heat generation in the stack is low, and therefore the stack airflow required for cooling is low. When the airflow through the stack itself is low, the minimum fresh airflow limit is reached at relatively low values of the air recirculation ratio, and before the electric air preheating can be eliminated.

Air recirculation has significant positive effects on system efficiency for most operating points. Without air recirculation (or an afterburner), some operating points are unable to provide positive net power, despite heat integration. This typically occurs at high current densities, low stack temperatures and high stack pressures. At such inefficient operating points, a large airflow is required for stack cooling. But because of high pressure, the air compressor has a high outlet temperature, while the outlet temperature of the air turbine is low. This makes heat integration difficult/impossible and large amount of electric heating is needed, leading to net negative power output. In these cases, air recirculation makes it possible to get moderately high positive efficiencies without needing an afterburner to provide heat. The largest efficiency improvement from air recirculation is seen at the operating point ($650\,^{\circ}\mathrm{C}$, $7.5\,\mathrm{bar}$, $7500\,\mathrm{A\,m^{-2}}$)[3], where the efficiency is increased from 4.9% to 59.6%, an increase of 54.7 %-points. However, air recirculation does not significantly benefit operating points that are already efficient. With optimal use of air recirculation, the maximum efficiency in FC mode increases from 76.1% to only 77.7%.

4.3. Electrolyser mode results

When electrolysis is exothermic, the effects of air recirculation in EL mode are nearly identical to FC mode, i.e. the optimum amount of air recirculation is the minimum amount which can ensure zero demand for electric air preheating.

However, the situation is different when electrolysis is endothermic, as shown in Fig. 4(b). In this situation, the (sweep) air input to the stack has to be heated up to $100\,^{\circ}\mathrm{C}$ above the stack outlet temperature. Since the maximum available temperature in the heat exchanger network is only the stack outlet temperature, fresh air cannot be heated to the required temperature by heat integration alone. Therefore, unlike FC mode, the exergy destruction from electric heating never becomes zero. It continues to decrease with increasing air recirculation, and reaches its minimum only when the fresh air inflow becomes zero and all the sweep flow comes from air recirculation (which, in this case, becomes recirculation of pure oxygen).

The inlet and exhaust air flow rates decrease with increasing recirculation, to maintain the air flowrate through the stack as explained previously. The exergy losses in the air turbomachinery also reduce with increasing air recirculation, since the flow rate through the turbine and compressor is reduced, and the fresh air compressor eventually becomes redundant. As the exhaust airflow rate decreases with increasing recirculation, the exergy losses to the environment also decrease. There is a slight increase in losses to the environment when the fresh airflow becomes very low. This is because the exhaust air becomes pure oxygen, increasing the chemical exergy lost to the environment. For all these reasons, the optimum air recirculation for endothermic electrolysis is the point when all the required input air is taken only by recirculation of the air exhaust. This also means that all the air-side flows in the system actually consist of pure oxygen rather than air.

Like FC mode, the largest efficiency improvement is observed at high stack pressures, since the heating effect of the compressor and the cooling effect of the air turbine hinder heat recovery, which is mitigated by air recirculation. At operating points where the airflow required for stack thermal management is high, the losses in electric heating and turbomachinery are high if no recirculation is used. Therefore, the efficiency benefit of air recirculation is the highest at these points. In EL mode, this is at the most endothermic operating point ($800\,^{\circ}\mathrm{C}$, $10\,\mathrm{bar}$, $2500\,\mathrm{A\,m^{-2}}$), where the use of air recirculation increases the efficiency by 30.0 %-points, from 49.1% to 79.1%. Similar to FC mode, air recirculation does not significantly benefit operating points that are already efficient. The maximum EL mode efficiency only changes from 78.4% to 79.2%.

4.4. Air recirculation summary

For most operating points (i.e. a combination of stack temperature, pressure and current density), there exists a single optimal value of air recirculation ratio that provides the maximum system efficiency, which usually corresponds to the need for electric air preheating being eliminated. In cases where the electric air preheating is already unnecessary, such as with near-atmospheric pressure FC operation, the optimal air recirculation remains zero. In some cases in FC mode (low current density, high temperature, high pressure), electric air preheating cannot be eliminated and the air recirculation is chosen to be at the oxygen starvation limit. On the other hand, for endothermic electrolyser mode, the optimum air recirculation value is that which eliminates all fresh airflow. For all further analyses, such an optimal value of the air recirculation ratio is used for each operating point.

Assuming that the amount of charge transferred through the system in each mode is equal, the RTE can be defined as the product of efficiencies of both modes. Without air recirculation, the RTE varies between 0%-52.8% for various rSOC operating points. Optimal use of air recirculation raises the RTE range to 37.7%-60.3%. The variation of efficiencies within this range based on rSOC operating parameters is discussed in Section 5.

5. Optimisation of rSOC system for highest efficiency

This section discusses the optimisation of rSOC operating points for highest round-trip efficiency. The optimised parameters for ammonia synthesis from Section 3, and the optimised air recirculation ratios from Section 4 were used in the simulations. For both FC mode and EL mode,

---

[3] There are also two operating points where the efficiency increase from air recirculation is hypothetically even larger. However, these points are not considered here, because they have a negative efficiency without air recirculation, making it difficult to meaningfully define efficiency improvement.

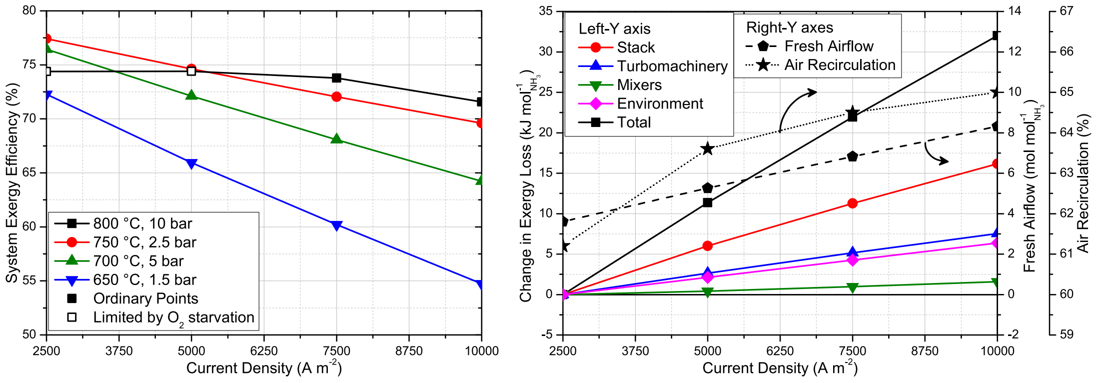

(a) FC mode: Variation of system exergy efficiency.

(b) FC mode: Difference in exergy losses, datum at 2500 A m^{-2}. Stack operating point for this example: 700 °C, 5 bar.

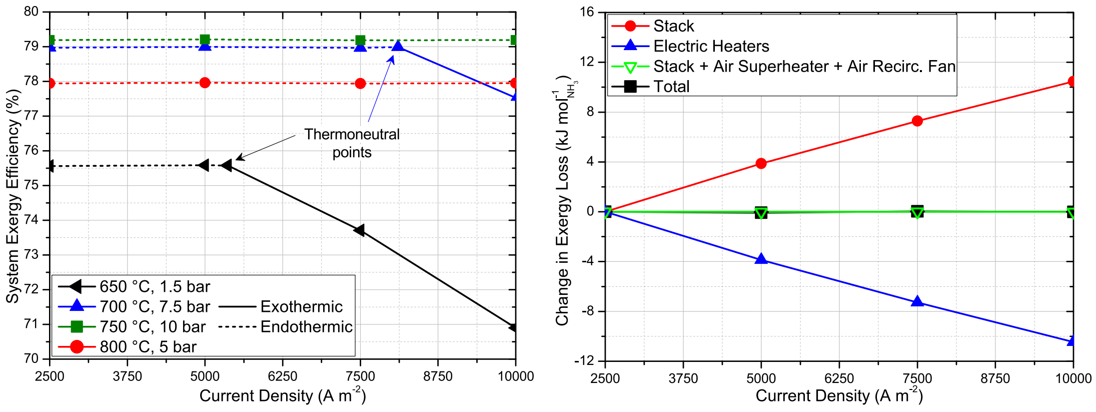

(c) EL mode: Variation of system exergy efficiency.

(d) EL mode: Difference in exergy losses, datum at 2500 A m^{-2}. Stack operating point for this (endothermic) example: 750 °C, 10 bar.

Fig. 5. Variation of rSOC system performance with current density.

the 80 operating points mentioned in Section 4.1 were tested. These were used to study the effect of each operating parameter in detail. Finally, assuming that the values of the parameters should be same in FC and EL modes, the optimal set of parameters was found for highest round-trip efficiency.

5.1. *Effect of current density*

5.1.1. *Fuel cell mode*

In almost all the cases considered in the present work, an increase in current density leads to a fall in system exergy efficiency in FC mode. Some of these cases are shown as an example in Fig. 5(a), and the exergy analysis explaining this trend is shown in Fig. 5(b). Note that as mentioned in Section 2.5, the exergy loss and mole flow rates in the analysis below are all normalised by ammonia mole flow rate for easier comparison between different current densities.

A linear increase in (normalised) stack exergy destruction is the biggest driving force behind the fall of efficiency, as overpotentials have a strong linear dependence on current density (the selected range of current density is in the linear “Ohmic” region of the FC polarisation curve). Therefore the (normalised) cooling airflow through the stack increases linearly with current density. This increased airflow requirement can be met either through an increase in the fresh airflow, or through an increase in the air recirculation ratio. As seen in Fig. 5(b) however, it is observed that both of these have to be increased together for optimum efficiency at each current density. Looking at Fig. 1(b), the high-temperature air preheating is handled by HEX4 using fuel electrode exhaust. The (normalised) flow rate of the fuel electrode exhaust (i.e. hot stream of HEX4, with lower heat capacity) is constant, while the (normalised) fresh airflow rate (i.e. cold stream of HEX4, with higher heat capacity) is expected to increase with current density. Therefore the outlet temperature of the HEX4 cold stream is expected to decrease with an increase in current density. This means the heat integration network becomes less effective at higher current density. In order to mitigate this and avoid electric heating, the optimum air recirculation is higher, since increased air recirculation also decreases the required outlet temperature of HEX4. This way, the heat integration network can handle a slightly higher flow of fresh air without electric heating. This is why both the optimum fresh airflow and the optimum air recirculation increase with higher current density. A higher fresh airflow naturally implies a larger exhaust airflow too, and thereby larger exergy destruction in air-side turbomachinery and larger exergy losses to the environment through the air exhaust. Higher air recirculation ratio also leads to larger exergy destruction in the air recirculation mixer. Larger airflows also lead to larger heat transfer and larger exergy destruction in the heat exchangers, especially HEX3 (although this is negligible in comparison to the other components and hence not shown in Fig. 5(b)). All these reasons are responsible for the drop in system efficiency.

In Fig. 5(a), it may be noticed that the graph of (800 °C, 10 bar) defies the linear trend. This is because the points relating to 2500 A m^{-2} and 5000 A m^{-2} are at the oxygen starvation limit described in Section 4.2, and thus have an efficiency lower than the expected linear values. This is solely due to non-zero electric air preheating demand and the associated increase in exergy destruction. Exergy losses in all other components vary as expected.

5.1.2. *Electrolyser mode*

The effect of current density in EL mode is shown in Fig. 5(c), for both exothermic and endothermic regions. In the exothermic mode, the

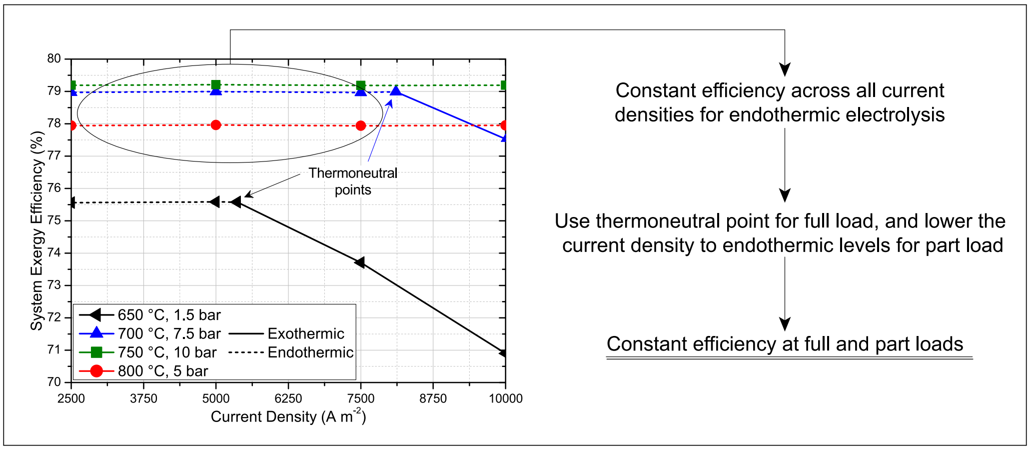

Fig. 6. Novel finding of this work: nearly constant electrolyser efficiency at full and part load.

system efficiency decreases linearly with rising current density, just like the FC mode. This is for the same reasons, driven mainly by increasing overpotentials and increasing airflow required to get rid of the excess heat. The endothermic region shows an unusual result. Usually, it is expected that increasing the current density in endothermic region improves the efficiency, since growing overpotentials move the stack towards thermoneutrality, reducing the airflow required and hence reducing the losses associated with the airflow.

However, it can be seen from Fig. 5(c), that the efficiency in the endothermic region is completely independent of current density, and equal to the maximum efficiency at the thermoneutral point for each pressure and temperature. This is because, as explained in Section 4.3, the optimal air recirculation in endothermic region maintains the fresh airflow at zero. Therefore, the conventional explanation associated with varying airflow does not apply to this system. This independence of efficiency with current density can be explained through an exergy balance.

Explanation of independence from current density

As explained before, the energy, exergy and material flow rates are all normalised by ammonia flow rate in order to easily compare between different current densities, and further references to these quantities in the next paragraph are to be taken as normalised even when not explicitly stated.

Note that most of the flow rates and process parameters in the system are independent of current density. Therefore, the exergy destruction in most of the components is independent of current density. The only exceptions to this are the components related to the recirculated air, which depend on the heat demand of the stack. Therefore, for the exergy balance, this is the only relevant part of the system. A temporary imaginary system boundary can be drawn including only the following components in Fig. 2(a): rSOC stack, air splitter, air recirculation fan, and air superheater (air mixer does not exist at zero fresh airflow). The incoming exergy flows crossing this boundary include: the fuel electrode inlet flow (E104), and the electric power inputs of the stack, air superheater, and recirculation blower. The outgoing exergy flows for the system boundary include: the fuel electrode exhaust (E201) and the air electrode exhaust (E602). All the material flow rates crossing the boundary are independent of current density, as are their corresponding exergy flows. Regarding the electric power inputs, the sum of the power inputs of the stack, air superheater and air recirculation fan, corresponds to the reaction enthalpy of steam electrolysis. This is also independent of current density. Therefore all the exergy flows crossing the temporary system boundary are independent of current density. This means that the (normalised) exergy destruction within this temporary boundary is also independent of current density. Therefore, the exergy destruction in the entire system is also independent of the current density for endothermic electrolysis. This can also be seen in Fig. 5(d). At higher current density, the stack exergy destruction is higher due to high overpotentials, however, the exergy destruction associated with electric heating in the air superheater reduces by the same amount, leading to the total exergy destruction in the system to be constant. Changes in exergy destruction in the recirculation fan are negligible.

The independence of endothermic electrolyser system efficiency from current density seen in Fig. 5(c) is the main novel finding from this work. This finding can be used to design electrolysis systems with nearly constant efficiency over the entire load range. This strategy is summarised in Fig. 6, and discussed further in Section 6.

5.2. Effect of stack temperature

5.2.1. Fuel cell mode

The effect of stack temperature is shown in Fig. 7, for the FC mode. It can be seen from Fig. 7(a), that the general trend of system exergy efficiency with rising stack temperature is upward. This is found to be the case for all operating points where the oxygen starvation limit is not reached (hereafter called “ordinary” points). The reason for this monotonic rise in efficiency can be further understood from looking at the ordinary points in Fig. 7(b), which shows the variation of exergy losses in various processes.

The largest reduction in exergy losses with temperature comes from the stack itself. Raising the stack temperature increases the operating voltage of a FC and reduces heat generation, due to greatly reduced overpotentials. Therefore, the exergy destruction in the stack associated with overpotentials and heat generation goes down significantly. Lower heat generation also means lesser cooling airflow through the stack. This could be achieved either by lowering the fresh airflow or lowering the air recirculation ratio. It can be seen from Fig. 7(b), that for ordinary points, the optimum air recirculation ratio actually increases with temperature (and thus the fresh airflow reduces even more). This can be explained by investigating heat exchanger HEX4 (in Fig. 1(b)). As the stack temperature is increased, the preheat requirement of the fresh air increases, and the heat availability from the fuel electrode exhaust also increases. However, since the heat capacity of the hot side of HEX4 (fuel electrode exhaust) is lower than the cold side (fresh air), the increase in actual heat transfer in HEX4 is less than the increases in heat availability or heat requirement. This means, the heat integration network is less effective at higher temperatures. Therefore, the optimum air recirculation ratio has to be higher at higher temperatures. Because of this, the fresh airflow reduces significantly. Since the fresh airflow is lower at higher temperatures, the exhaust airflow is lower as well. The exergy destruction in the air-side turbomachinery reduces due to the lower flow rates, as does the exergy loss to the environment via

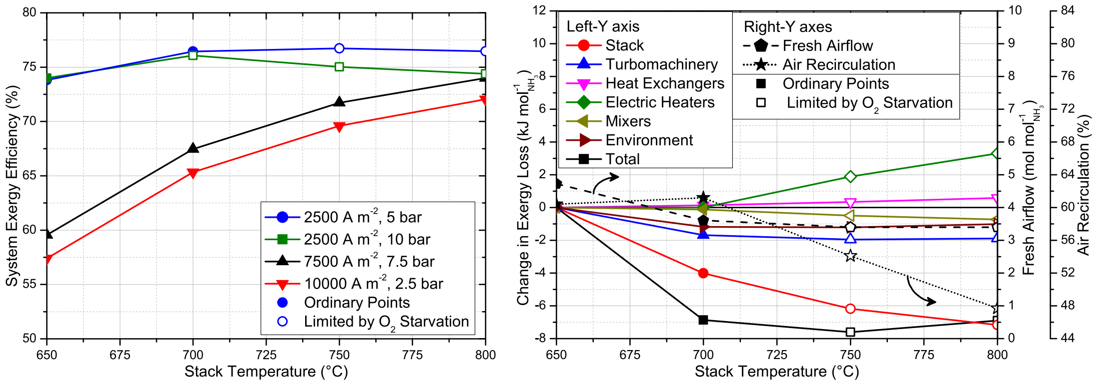

(a) FC mode: Variation of system exergy efficiency.

(b) FC mode: Difference in exergy losses, datum at 650 °C. Stack operating point for this example: 2500 A m^{-2}, 5 bar.

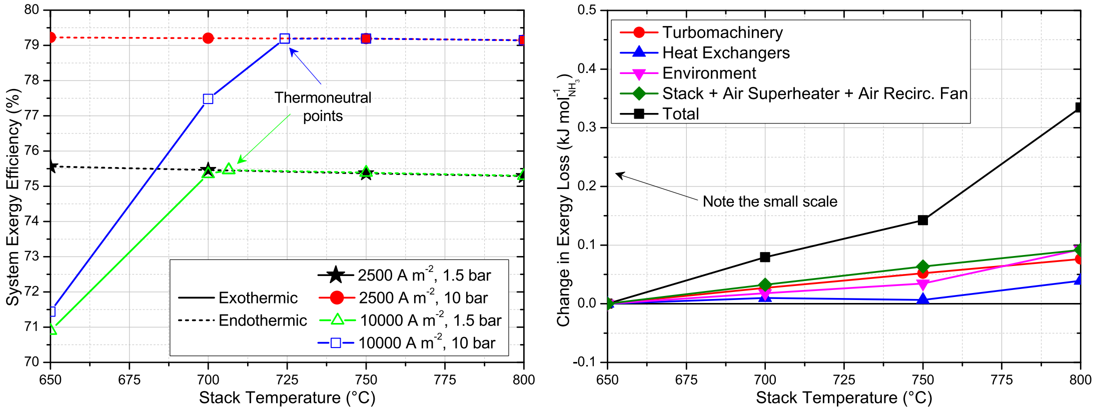

(c) EL mode: Variation of system exergy efficiency.

(d) EL mode: Difference in exergy losses, datum at 650 °C. Stack operating point for this (endothermic) example: 2500 A m^{-2}, 10 bar.

Fig. 7. Variation of rSOC system performance with stack temperature.

the exhaust. At high stack temperatures, higher temperature differences in the heat exchangers also lead to slight increases in the exergy destruction despite lower heat transfer rates.

However, as mentioned previously, there are a few operating points where the oxygen starvation condition has been reached, and these are also depicted in Fig. 7(a). In cases where oxygen starvation limit is reached, increasing the stack temperature any further causes a decrease in the system efficiency. The reasons for this are as follows, also seen in Fig. 7(b). The primary reason is the rapid rise of exergy destruction associated with electric heating. At points of oxygen starvation, the fresh airflow is as low as it can be. But as explained in the previous paragraph, the heat integration network gets less effective at higher stack temperature. Since the airflow cannot be reduced further, this causes a shortage of heat for preheating, which has to be met through electric heating, leading to a rise in exergy destruction. Now, the fresh airflow is at its minimum, but the cooling demand of the stack reduces further as temperature is increased. Therefore, the airflow through the stack is reduced by reducing air recirculation, and the exergy destruction in the air mixer reduces due to reduced recirculation. Since the fresh airflow and exhaust airflow are now constant at their minimum levels, the previously downward trends of exergy destruction in turbomachinery and exergy loss to the environment through air exhaust also flatten out. Further, the fuel electrode exhaust is at a higher temperature, but the heat transfer in HEX4 is limited due to the relative heat capacities of the flow. So the additional thermal exergy is lost to cooling water through the steam condenser, which means losses to the environment start to increase. Oxygen starvation does not affect exergy destruction in heat exchangers, which continues to rise slightly due to higher temperature differences caused by higher stack temperature. These things together lead to an increase in total exergy losses, driving down the system efficiency for points with oxygen starvation.

5.2.2. Electrolyser mode

The effect of stack temperature in EL mode differs widely based on whether the stack is endothermic or exothermic. Both the endothermic and exothermic regions are depicted in Fig. 7(c). In the exothermic region, the effect of temperature is similar to the effect seen in the FC mode. The system efficiency increases with a rise in stack temperature, driven mainly by reduction in exergy destruction in the stack, air-side turbomachinery, and exergy losses through the exhaust airflow.

In the endothermic region, the effect of temperature on exergy destruction is similar to the effect of current density, due to the high air recirculation approach. The changes in exergy destruction in the stack and air superheater almost (but not entirely) negate each other. Unlike the current density case, the sum of exergy destruction in the two components rises slightly with stack temperature as shown in Fig. 7(d). These changes are not very large, and the resulting decline in efficiency is rather small (< 0.5%-points), but it is consistent/monotonous enough not to be attributed to rounding errors or other numerical artefacts. The reasons for these changes are as follows.

The total enthalpy change of the reaction represents the conversion of electrical energy into chemical or thermal energy, which takes place in the stack, air superheater, and air recirculation fan. The enthalpy change of the electrolysis reaction increases slightly with temperature. Since the energy conversion overall increases slightly with stack temperature, the associated exergy destruction (in the stack, air superheater and air recirculation fan) also increases slightly with temperature.

There are also slight increases in exergy lost in other components as the stack temperature is increased. The exergy destruction in heat exchangers rises slightly because more heat is transferred to bring steam to higher stack temperatures. Further, the rising stack temperature

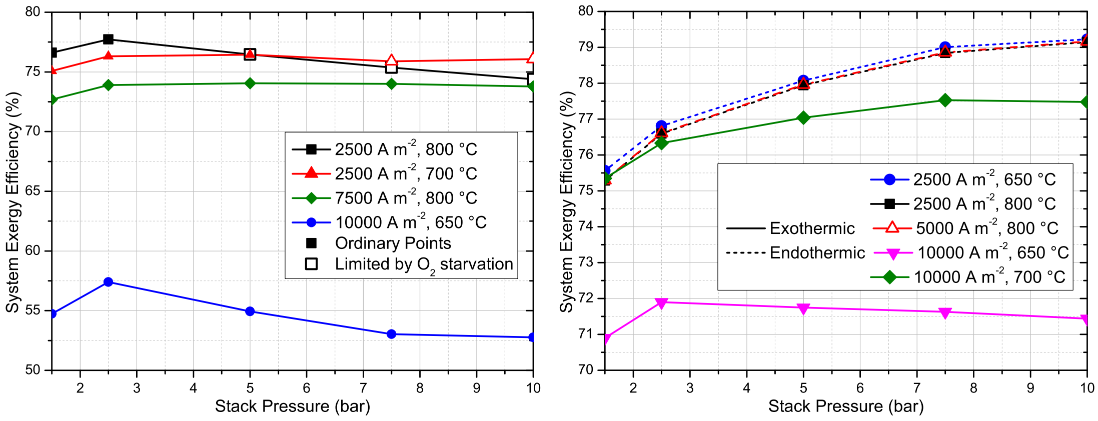

(a) Fuel cell mode.

(b) Electrolyser mode.

Fig. 8. Variation of system performance with stack pressure, datum at 1.5 bar.

changes the temperature profiles in the heat integration network, such that slightly less heat can be extracted from the hydrogen compression intercoolers. This increases the exergy loss to the environment through cooling water.

5.3. Effect of stack pressure

5.3.1. Fuel cell mode

Unlike the other two stack parameters, the stack pressure is not observed to have a monotonic effect on the efficiency of the system in FC mode. As seen in Fig. 8(a), the system efficiency peaks somewhere within the tested pressure range, and then drops as pressure is increased further. The exergy analysis for this variation is shown in Fig. 9(a), and elaborated in the following paragraphs.

The exergy destruction in the stack consistently decreases with rising pressure. This is mainly because of a reduction in exergy destruction in the ammonia cracking process that occurs within the stack. Additionally, the cell voltage is higher at higher pressure, driven mainly by reversible voltage. This leads to lower heat generation in the stack, but does not affect the exergy destruction since the overpotentials (i.e. irreversible part of heat generation) do not noticeably change.

Air preheating through the heat integration network is less effective at higher stack pressure, for the following reasons. The air electrode exhaust passes through the air turbine before entering the heat integration network, while the cold air entering the network comes from the air compressor. Because of this, the temperature of hot air stream entering HEX3 (Fig. 1(b)) goes down when stack pressure is increased, while the temperature of the cold air entering in HEX3 rises. This causes a significant drop in heat transfer in HEX3, which is only partially counteracted by a rise in heat transfer through HEX4. Since the overall air preheating possible in HEX3 and HEX4 is reduced at higher pressure, the air recirculation has to be increased sharply in order to reduce the preheating demand and avoid using electric heating. For the example shown in Fig. 9(a), the optimum air recirculation ratio goes from 6% at 1.5 bar to as high as 72% at 10 bar.

Increased air recirculation causes an increase in exergy destruction in air mixing. The significantly reduced heat transfer in HEX3 also reduces the total exergy destruction in heat exchangers. The air exhaust temperature also increases due to reduced heat recovery in HEX3. Due to the reduction in stack heat generation, as well as the sharply increased air recirculation (as explained in the last two paragraphs), there is a steep fall in amount of fresh airflow.

All the effects mentioned above are greatest at the lower pressure ranges (<2.5 bar), and become less stark at higher pressures. This is because a small absolute change in stack pressure represents a proportionally larger change in pressure ratio in the turbomachinery when the stack pressure is low. Hence the outlet temperatures of the air turbine and compressor change the fastest at lower pressures. Therefore the reduction in heat transfer possible in HEX3 is also the most significant at low stack pressures, as are all the changes resulting from this, which are described in the previous paragraphs. At low pressure ranges, the exergy loss to the environment through the air exhaust also drops (despite increasing exhaust temperature) due to the greatly reduced fresh and exhaust airflows.

At higher pressures (>2.5 bar), the effect of pressure rise is smaller, since the same absolute rise in stack pressure represents a proportionally smaller rise of pressure ratio in the turbomachinery when the stack pressure is high. Moreover, the increase in air recirculation reduces the target temperature for air preheating, meaning that the heat integration network can preheat slightly larger fresh airflows with the available heat. Hence, the reduction in fresh airflow also becomes much less steep, and other factors apart from air flowrate start to dominate. Notably, the exergy loss to the environment through the air exhaust increases. As mentioned before, the reduced heat recovery in HEX3 raises the air exhaust temperature. Since the reduction in air flowrate is less steep, the rising exhaust temperature causes a rise in exergy lost through the exhaust.

The variation of exergy destruction in turbomachinery is more complicated. On one hand, the exergy destruction in the nitrogen-hydrogen compressors reduces at higher stack pressure, simply due to the reduction in pressure ratio between the ammonia synthesis system and the stack. On the other hand, the exergy destruction in the air compressor and turbine increases due to the increase in pressure ratio between the stack and the atmosphere. Among these two effects, the effect of the air turbomachinery usually dominates, since the flow rates of air are typically much higher than the fuel side flows, and the air-side machinery is single stage, compared to the multi-stage nitrogen-hydrogen compressors. Therefore, in most cases the total exergy destruction in turbomachinery usually increases with stack pressure, but this is not always true (like in Fig. 9(a)). This can also get further complicated since the airflow rate varies greatly with pressure. In the particular example shown in Fig. 9(a), the two contrasting effects seem to cancel out almost entirely.

Interestingly, between 7.5 bar and 10 bar, the exergy destruction in the heat exchangers increases while the loss to the environment decreases. This is because at ~8.5 bar, the boiling point of ammonia crosses 20 °C, and the heat of evaporation of ammonia starts being provided through the heat integration system rather than from the environment. The sum of these two continues to increase, however, therefore the overall efficiency trend is unaffected by this switch.

To summarise the analysis of Fig. 9(a), as the stack pressure increases, the exergy destroyed in stack and heat exchangers decreases, while exergy destroyed in mixing and lost to the environment increases. Due to the interplay between these opposing effects, the optimum

Table 1
Summary of sensitivity analysis: how each parameter affects the system exergy efficiency in each mode.

Operating parameter	FC mode	Endothermic EL Mode	Exothermic EL mode
Air Recirculation ↑	↷	↗	↷
Current Density ↑	↘	→	↘
Stack Temperature ↑	↗	→	↗
Stack Pressure ↑	↷	↗	↷

pressure lies at an intermediate value. In general among the 80 points tested, the optimum pressure varies between 2.5 bar and 5 bar based on the other operating parameters.

In Fig. 8(a), the line for 650 °C shows a slowdown in the decline of efficiency between 7.5 bar and10 bar. This is because at low temperatures and high pressures, HEX3 becomes entirely inoperative. After this point, a major drawback of high pressure (i.e. the reducing heat recovery in HEX3) disappears. Any further increase in stack pressure (and thus temperature of air at the compressor outlet) now increases the inlet temperature of HEX4, which can therefore heat a higher airflow. This allows a reduction in air recirculation. Since HEX3 is no longer active, the air exhaust temperature now equals the outlet temperature of the air turbine, which reduces with rising stack pressure. This also reduces the losses to the environment. However, larger fresh airflow and higher pressure leads to increased exergy destruction in turbomachinery, which is why the efficiency still reduces between 7.5 bar and 10 bar, albeit slightly. What may happen to this system at even higher pressures remains to be investigated in the future.

In Fig. 8(a), it can also be seen that oxygen starvation does not affect the general shape of the curve. The optimum pressure is moved to a lower value, and the exergy destruction of electric heating (which cannot be reduced any more) leads to a sharper decline in efficiency than usual. The trends of exergy losses in other components remain largely the same as the ordinary cases. But air recirculation reduces in order to reduce the airflow through the stack while fresh airflow is constant at its minimum. Exergy destruction in the air mixer follows the trend of the recirculation.

Finally, Fig. 8(a) also visually demonstrates the point that oxygen starvation tends to hinder the system at some of its highest efficiency points. This is because stack efficiency is a major determinant of system efficiency (both directly, and through its effect on cooling airflow), and oxygen starvation is an issue only when the stack is already very efficient, as was explained in Section 4.2.

5.3.2. *Electrolyser mode*

In Fig. 8(b), the trends of system exergy efficiency with stack pressure are shown, for both endothermic and exothermic regions. In the exothermic region, the efficiency shows trends similar to FC mode, with an optimum intermediate pressure (in this case between 5 bar and 10 bar). A comparison of Figs. 9(a) and 9(b) shows that the general trends of exergy destruction, airflow and recirculation are very similar to the FC mode. To recap, the increased pressure ratio causes an increase in air compressor outlet temperature, and decrease in the air turbine outlet temperature. This causes a reduction in possible heat transfer in the air–air heat exchanger (HEX9 in Fig. 2(b)), reducing the amount of fresh airflow that can be preheated. Thus the fresh airflow has to be reduced by increase the air recirculation.

The increased recirculation increases the air mixing losses. The lower heat recovery in HEX9 increases the air exhaust temperature, thus increasing the exergy loss to the environment. The exergy destruction in heat exchangers is led by two factors. Firstly, the reduced heat transfer and temperature differences in HEX9 reduces exergy destruction in heat exchangers. Secondly, the increased boiling point of water at higher pressures also reduces the average temperature differences in some of the water-evaporating heat exchangers. Both these factors together lead to a large drop in overall exergy destruction in heat exchangers. Lastly, as mentioned in the FC mode section, the exergy destruction in turbomachinery usually rises with pressure, which is true for the case shown in Fig. 9(b).

The main difference between the effects of pressure on FC mode and EL mode is in the rSOC stack. In FC mode, the large variation in stack exergy destruction is attributed to ammonia cracking, which is not present in steam electrolysis. The stack pressure only affects the reversible voltage of an rSOC, while the overpotentials are affected very weakly in the Ohmic region of operation. Therefore, the exergy destruction in the stack in EL mode has negligible variation with pressure.

The observations from Sections 5.1.2 and 5.2.2 regarding the endothermic region are also seen again in Fig. 8(b). That is, the curves for different current densities but same stack temperature (i.e. the red and black curves) overlap perfectly, whereas the curves for same current density but different temperature (i.e. the blue and black curves) vary only slightly from each other. This confirms that the endothermic system efficiency is independent of current density, and weakly dependent on temperature. It is also clear from Fig. 8(b) that the effect of stack pressure on endothermic electrolysis is different from that of temperature or current density, i.e. the endothermic system efficiency is not constant, but actually increases with stack pressure.

This is explained using Fig. 9(c). As explained previously, the optimum fresh airflow is zero for each endothermic operating point. As the stack pressure is increased, the cell voltage increases (led by an increase in reversible voltage) and hence the stack becomes less endothermic. Therefore, the heat provided via electric air superheating decreases, and the exergy destruction associated with this electric heating decreases. In case of temperature or current density variation, this reduction in exergy destruction would be matched by a corresponding increase in exergy destruction in the stack. But stack losses in electrolysis are only weakly dependent on pressure, as explained before. Therefore, the reduction in electric heating exergy destruction is not nullified by an increase in stack exergy destruction, and the sum of losses in the stack and air recirculation loop actually decreases with rising stack pressure. Further, increasing stack pressure also reduces the losses in turbomachinery, due to lower hydrogen compression needs. Since the fresh airflow is zero, there is no increase exergy destruction in the air compressor. There is a rise in exergy destruction in the air turbine at higher pressures, but this is negligible because the air exhaust flow is small due to zero fresh airflow. The exergy destroyed in heat exchangers reduces with rising stack pressure as well. At higher pressure, the average temperature difference in water evaporating heat exchangers is smaller due to higher boiling point of water. Further, the latent heat of water is also smaller at higher pressure. Therefore, the exergy destruction in heat exchangers reduces significantly. The exergy lost to the environment decreases with increasing stack pressure as well, because at higher pressure ratios, the air turbine can recover more exergy from the exhaust. All these reasons cause the total exergy losses in endothermic region to decrease with rising stack pressure, improving the efficiency.

5.4. *Optimum operating points for round-trip efficiency*

Table 1 summarises the sensitivity analysis from the previous sections by showing how each parameter affects the efficiency in each mode. After having carried out the sensitivity analysis for 80 operating points, the optimum operating point from among these can be selected.

In FC mode, it has been shown that low current density is always beneficial for efficiency, while the stack temperature should be the highest value possible, as long as the oxygen starvation limit is not reached. On the other hand, the optimum stack pressure values are between 2.5 bar and 5 bar, with the exact value depending on the other parameters. As a combination of these effects, it is found that the optimum operating point for FC mode is (2500 A m^{-2}, 800 °C, 2.5 bar), with a system exergy efficiency of 77.7%.

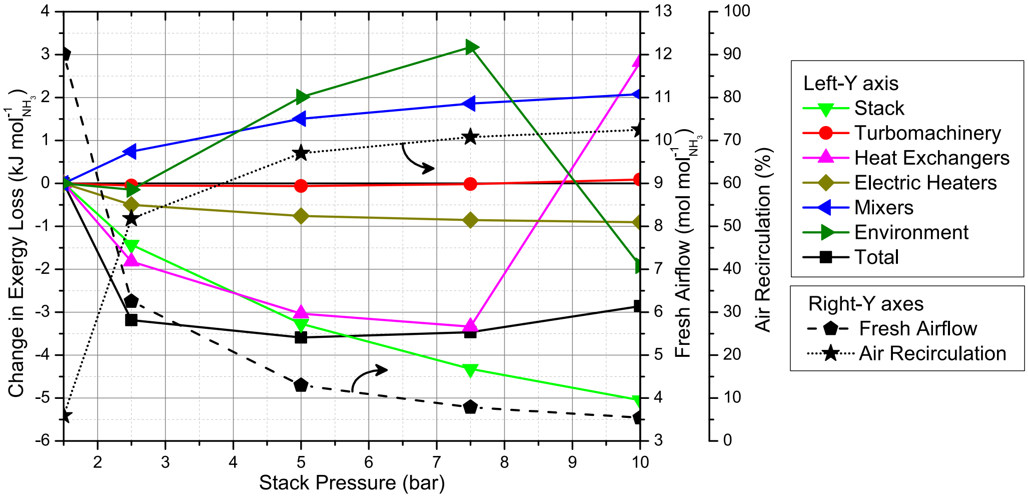

(a) Fuel cell mode. Stack operating point for this example: 7500 A m^{-2}, 800 °C.

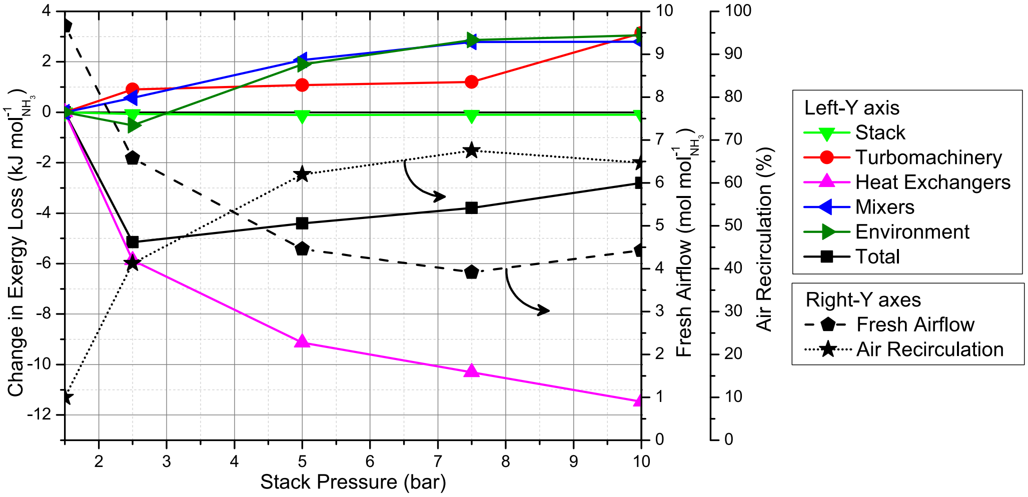

(b) Exothermic electrolyser mode. Stack operating point for this example: 10 000 A m^{-2}, 650 °C.

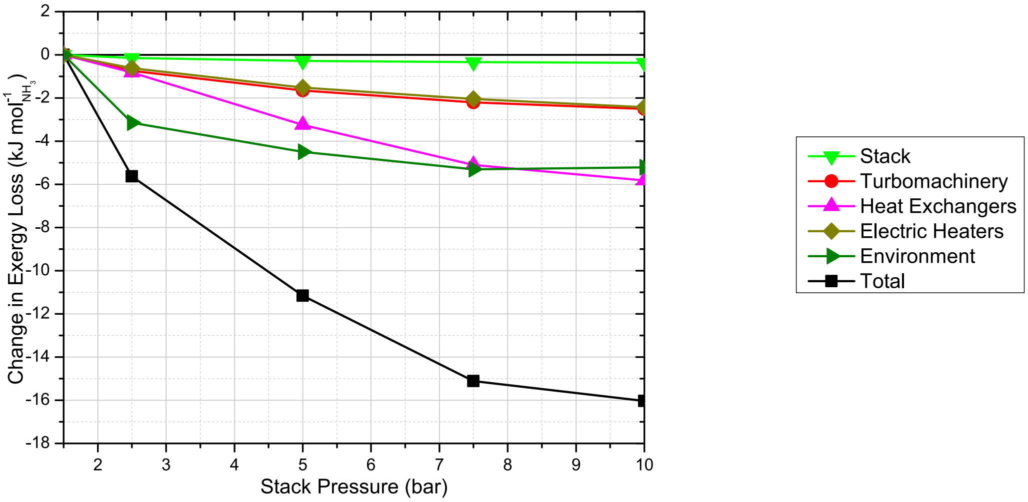

(c) Endothermic electrolyser mode. Stack operating point for this example: 2500 A m^{-2}, 650 °C.

Fig. 9. Differences in exergy losses with stack pressure, datum at 1.5 bar.

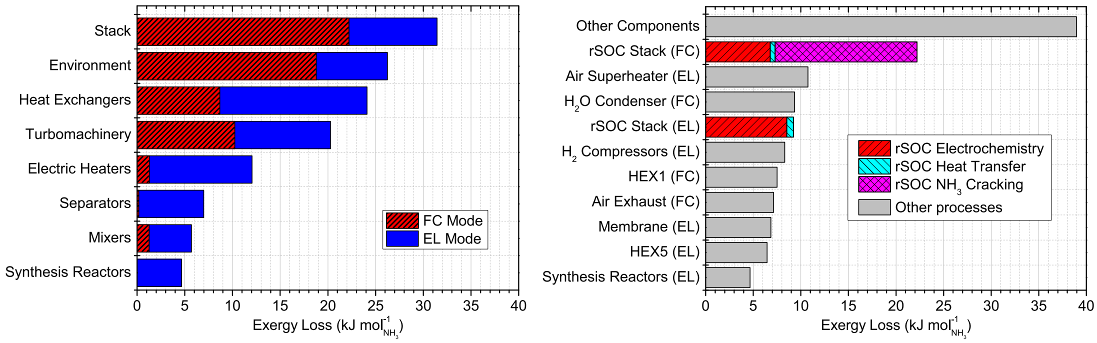

(a) Process-wise loss distribution (b) Ten components with the highest losses

Fig. 10. Distribution of exergy losses in the optimised system.

In EL mode, it has been shown that the endothermic region is more efficient than the exothermic region in every case. Higher stack pressure is favourable for all endothermic cases. Further, current density is of nearly no consequence, as long as the electrolysis remains endothermic. And while the optimum stack temperature is the one corresponding to a thermoneutral point, a higher choice of temperature only applies an almost negligible efficiency penalty. Because the current density and stack temperature are of so little consequence, it is found that there are several optimum operating points for the EL mode, with system exergy efficiency of approximately 79.2%. Apart from them being in the endothermic region, the only parameter these points have in common is a stack pressure of 10 bar.

However, this study assumes that the stack temperature, pressure and current density are the same for each mode. Therefore, the choice of optimum operating point has to be made based on round-trip efficiency. This point is found to be (2500 A m^{-2}, 700 °C, 10 bar), which attains a round-trip efficiency of 60.3%, as shown in Table 2. This point turns out to be the optimum for the round-trip, since the EL mode prefers higher pressures, but increasing the pressure at 800 °C in FC mode takes it into the oxygen starvation zone, which is avoided by reducing the temperature to 700 °C. The advantage of higher pressure in EL mode turns out to be larger (in this case) than the disadvantage of lower temperature in the FC mode. The maximum round-trip efficiency of this ammonia system is in the same range as that found by other similar studies that include detailed thermodynamic analyses, such as the methanol system studied by Giannoulidis et al. (64.3%) [17].

Lastly, while there is no techno-economic analysis carried out in this work, it is pertinent to note that using higher current densities may enable the use of smaller rSOC stacks, which is beneficial from a capital cost perspective. Therefore, it may be useful to take notice of the efficiency of this system at higher current densities. At a current density of 5000 A m^{-2}, the optimum round-trip efficiency reduces slightly to 59.4%, and reduces to 58.4% for a current density of 7500 A m^{-2}. But even at the highest current density studied in this work, i.e. 10 000 A m^{-2}, the round-trip efficiency still remains as high as 56.7%. This can be attributed to the high air recirculation, which makes electrolysis almost equally efficient at any current density, as long as the stack remains endothermic. Therefore any decline in round-trip efficiency is attributed largely to the FC mode.

5.5. Exergy analysis of the optimised system

The distribution of exergy losses in the system at the optimised operating point is shown in Fig. 10. Fig. 10(a) groups all components based on the type of process they carry out, as has been done in many graphs in previous sections. On the other hand, Fig. 10(b) focuses on the ten components/operations with the highest losses.

As seen in Fig. 10(a), the largest losses come from the rSOC stack, 31.44 kJ/mol$_{NH_3}$ in both modes combined. FC mode contributes a greater share of these losses (22.21 kJ/mol$_{NH_3}$) than EL mode (9.23 kJ/mol$_{NH_3}$). In EL mode, the exergy destruction in the rSOC stack itself is relatively small. However, it must be remembered that the electrolysis reaction also requires the heat provided by the air superheater. Therefore the overall exergy destruction related to the electrolysis reaction is actually 19.98 kJ/mol$_{NH_3}$. Providing heat to the electrolysis reaction through electric air heating involves significant losses, while the rSOC in FC mode operates in an exothermic manner. Therefore, there is a possibility for storing heat from the FC mode in high temperature thermal energy storage, and using that in the endothermic EL mode to reduce the air superheating losses.

Table 2
Operating point for optimum round-trip operation.

Operating parameter	Optimum value
Current Density	2500 A m^{-2}
Stack Temperature	700 °C
Stack Pressure	10 bar
Air Recirculation Ratio (FC mode)	59.2%
Air Recirculation Ratio (EL mode)	94.6%
FC mode efficiency	76.1%
EL mode efficiency	79.2%
Round-trip efficiency	60.3%

The largest contribution to the rSOC stack losses in FC mode comes from the internal ammonia cracking reaction which destroys exergy at the rate of 14.90 kJ/mol$_{NH_3}$. In contrast, in EL mode, the exergy destruction in the three ammonia synthesis reactor stages combined is only 4.66 kJ/mol$_{NH_3}$. Analysing this difference of exergy destruction in chemical reactions, and identifying its causes, is part of ongoing research.

The second highest exergy losses come from exergy released to the environment, mainly in FC mode. Both the steam condenser cooling and the air exhaust flow have similar contributions to this loss (9.35 kJ/mol$_{NH_3}$ and 7.14 kJ/mol$_{NH_3}$ respectively). The high stack pressure causes the heat recovery from these streams to be less effective, since the air compressor outlet temperature is over 330 °C. Therefore these two streams carry a significant amount of heat, but at relatively low temperatures (<150 °C and <300 °C respectively). While the air preheating is still partially electric, air recirculation cannot be increased further to eliminate this, as it is hindered by oxygen starvation. This, combined with the low temperature of the waste heat, means that there is no more scope to integrate this heat within the existing system. Therefore, the most promising way to reduce this loss would be to integrate a low-temperature bottoming power cycle like an organic Rankine cycle.

The third largest group of exergy losses come from heat exchangers. The main contribution to this is from the water evaporators in EL mode, which destroy a combined total of 14.13 kJ/mol$_{NH_3}$. This is because the latent heat of evaporation has to be provided by the sensible heat from several streams. This combination of latent heat and sensible heat in the same heat exchanger(s) means that the average temperature difference is rather high, leading to large irreversibilities in heat transfer. Similarly, in FC mode, the largest heat exchanger losses come from HEX1, which acts as an ammonia evaporator at stack pressures above ∼8.5 bar, when the boiling point of ammonia is too high for evaporation using ambient heat. These losses can only be reduced if latent heat streams at suitable temperatures are available. The steam condensers in either operating mode are possible sources of latent heat (and also one of the largest sources of exergy loss, as mentioned in a previous paragraph). Integration of these condensers with the evaporators can be explored. But the condensers are at a lower temperature than the evaporators (due to pressure losses throughout the system, the condensers operate at a lower pressure than the evaporators, which means a lower boiling point), therefore such integration would require a heat pump, or some electric heating. Moreover, using condenser heat from the FC mode for water evaporation in the EL mode would also require low temperature thermal energy storage. Additionally, the exergy that is currently recovered from sensible heat streams by heat integration will have to be recovered by other means (perhaps organic Rankine cycles).

Other components causing significant exergy destruction are the hydrogen compressors, the membrane separator (due to the large pressure ratio across the membrane), ammonia synthesis reactors, and the electric air preheater (which cannot be eliminated in this case due to oxygen starvation limit).

Exergy flow diagrams for the system in each mode are presented in Fig. 11.

6. Discussion

This work implements the optimum amounts of air recirculation needed for each operating point in both FC and EL modes. The use of air recirculation in FC mode allows for high efficiencies without the need for an afterburner to provide heat. This is useful for a reversible system where unutilised fuel from FC mode can be stored instead of combusted. Without an afterburner, some operating points in FC mode cannot be used, since they have negative efficiency due to lack of heat from the integration network. Air recirculation can provide the required heat and significantly increase the efficiency, thus enabling the use of these operating points, if so desired. The peak efficiency in FC mode is only increased by 1.6 %-points. But the largest observed efficiency improvement in FC mode is from 4.9% to 59.6%, an increase of 54.7 %-points. Such large improvements are observed mostly for points with high current density. Typically, high current density indicates low capital cost due to high yield per rSOC stack area, but also high operating cost due to low efficiency. By increasing efficiency, air recirculation can reduce the operating costs, making these operating points much more feasible.

In FC mode, high amounts of air recirculation are seldom used in literature because low oxygen concentration reduces the cell voltages [29]. Our study takes air recirculation to much higher levels, stopping just before the point where irreversible damage is reported in literature [63]. It is found that the reduced stack power output does not overturn the benefits of reduced compressor power and external heating that are offered by increasing air recirculation. With this finding, it becomes much more important to conduct further research to more precisely find out the lower limits of oxygen concentration that SOCs can safely tolerate in FC mode.

In EL mode, the results of this work recommend the use of no fresh sweep air, entirely using recirculated oxygen instead. There are some concerns with using high oxygen partial pressures, such as fire/explosion hazards [64]. However, several modelling and experimental studies with SOCs operate with pure oxygen at the air electrode, either via oxygen sweep [18,32,33,65] or with no sweep flow at all [34,66]. Furthermore, a recent experimental study has indicated operating with high oxygen partial pressures at the air electrode might mitigate degradation mechanisms compared with operation in air [67]. Therefore, we consider it feasible to recommend recirculated oxygen sweep for EL mode.

Apart from the efficiency improvement, producing pure oxygen can also improve the economics of the system [34] by adding another product with market value. Alternatively, for reversible systems such as this one, the oxygen can be stored and reused in FC mode [18], increasing the efficiency of FC mode and also removing the air recirculation limits found in FC mode due to oxygen starvation.

A novel and useful effect of oxygen recirculation for endothermic operating points of EL mode is also found in this work. In this situation, the system efficiency is almost entirely independent of current density. This enables a new approach for part-load EL operation. The stack can be sized for thermoneutral operation at nominal load, and for endothermic operation at part loads. Such a system will operate with almost constant efficiency throughout the load range. This is made possible because recirculation ensures that no excess air has to be drawn from the atmosphere, and thus no excess air is exhausted back into the atmosphere. Therefore, no part of the electric heat added in endothermic mode is lost to the environment. This is in contrast to systems using sweep air, which lose some of the added heat via the air exhaust. In those systems, this loss would depend on the amount of sweep air and hence on the current density.

However, it must be noted that there are some effects neglected in the present work, which could affect part-load efficiencies. This work neglects the heat losses from the rSOC stack surface. These heat losses can reduce the part-load efficiency, since the surface heat loss is constant at all loads (depending only on stack temperature), while the fuel production reduces with reducing load [40]. However, for large and well-insulated stacks in future large-scale systems, this effect can be expected to be relatively small. The effect of variations in efficiencies of compressors at part loads has not been considered in this work. These effects could be non-negligible for the compressors used for pressurising hydrogen and nitrogen to ammonia synthesis pressure. However, these effects could hypothetically be mitigated by introducing buffer tanks at strategic points in the process chain, so that the compressors can be sized to operate at a constant average load. The effect of varying compressor efficiencies could also be part of future studies. Similarly, mechanical losses from turbomachinery (i.e. bearing friction, etc.) are not recovered, which can also reduce the efficiency slightly. However, these are small enough to be negligible, and thus the efficiency at part-load can still be considered nearly constant.

Lastly, the use of electric heating plates for direct heating of the stack can also lead to a similar constant efficiency (if heat losses from stack surface are negligible), since there is no need for variable air sweep when using heating plates. However, as mentioned in Section 1.1, the use of heating plates in larger stacks might either cause temperature differences between cells or increase the design complexity. In contrast, air recirculation should be easier to implement and can be expected to result in more uniform temperatures in all cells. A comparison between the dynamic response of stacks with heating plates and stacks with air recirculation would also be an interesting line of future study.

Our optimised ammonia synthesis pressure of 170 bar is close enough to typical modern systems using promoted magnetite catalysts (∼150 bar) [68]. The small difference might be due to the use of a simple single-pressure synthesis loop rather than more complicated designs. There exist developments that can reduce further reduce the synthesis pressure and temperature, such as wustite or ruthenium catalysts, or adsorption-based ammonia separation. But more development is needed before efficiency gains from these methods can be assured [68]. In our optimised system, the hydrogen and nitrogen compressors consume $43.6\,\mathrm{kJ/mol_{NH_3}}$ power. But we also recover $48.8\,\mathrm{kJ/mol_{NH_3}}$ heat energy for steam generation. Reducing synthesis pressure (thus also temperature) might reduce heat recovery and lead to more electric heating. Therefore the effects of integrating lower-pressure ammonia

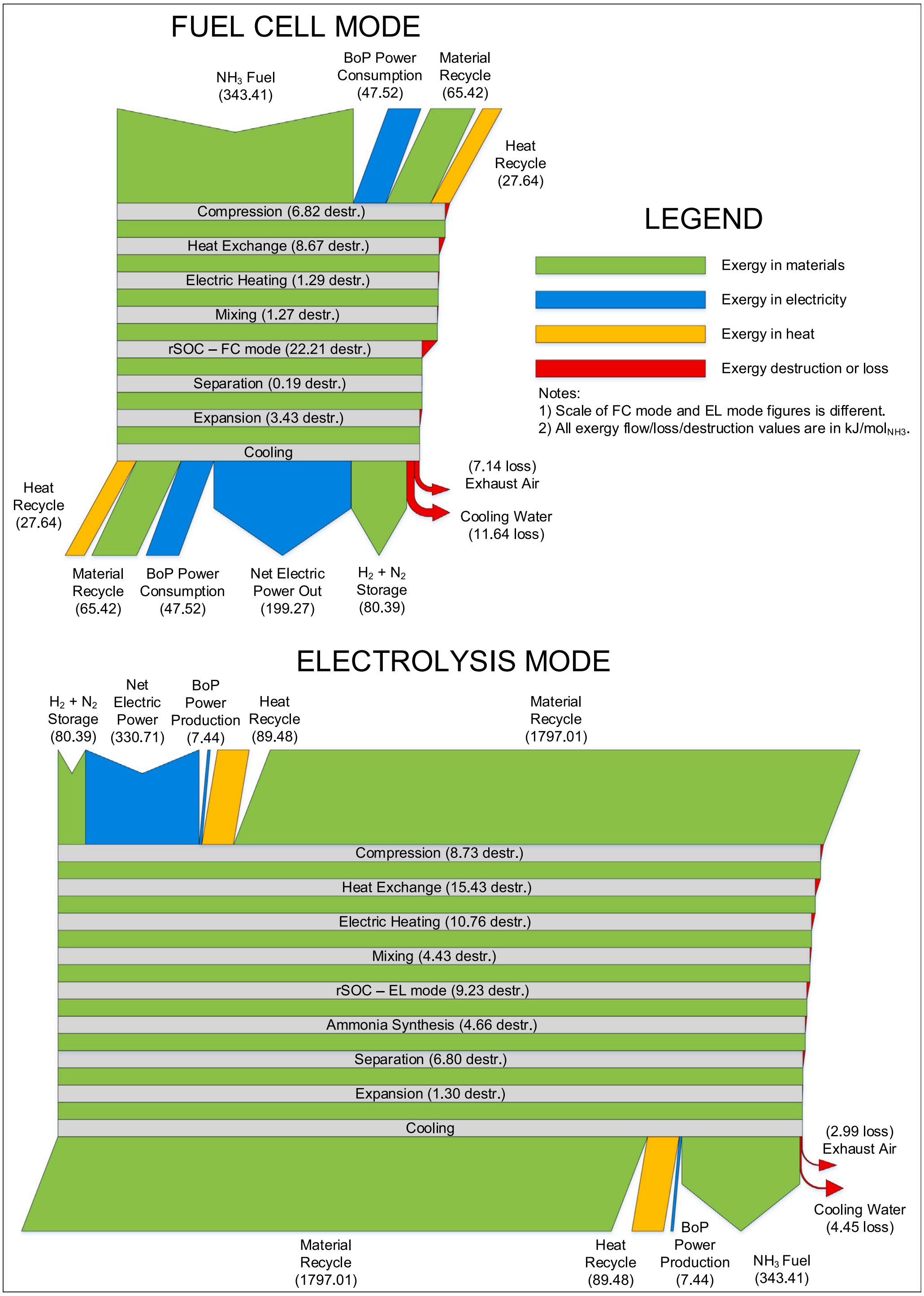

Notes:
1) Scale of FC mode and EL mode figures is different.
2) All exergy flow/loss/destruction values are in kJ/mol_{NH3}.

Fig. 11. Exergy flow diagrams at optimum operating point.

synthesis methods with rSOC systems is another area that needs further research.

The operating parameters of the rSOC stack and ammonia synthesis system are optimised to attain a DC-to-DC round trip efficiency of 60.3%. This efficiency is comparable to that found in other similar studies using fuels like methanol [17]. The optimum efficiency is attained at 700 °C stack temperature, 10 bar stack pressure (the highest value tested) and 2500 A m^{-2} current density (the lowest value tested). But even at higher current densities, the system achieves high efficiencies, for example 56.7% at 10 000 A m^{-2}, which is only a small decline compared to the optimum.

7. Conclusions

This work presents an efficient process design for an energy storage system which uses reversible solid oxide cells to store renewable electricity in the form of ammonia. The optimised system achieves DC-to-DC round-trip efficiencies of up to 60.3%. These findings are supported by an extensive exergy-based sensitivity analysis.

The results of this work confirm the benefits of air recirculation for rSOC systems described in literature, and suggest optimum amounts of air recirculation for operating in each mode. The novel finding of this work is that optimal air recirculation makes the efficiency of the endothermic EL system nearly independent of current density or temperature. This enables part-load EL operation with nearly constant efficiency. This is expected to be very useful in the future, where electrolysers running on intermittent renewables might frequently need to operate at part loads. In FC mode, optimal air recirculation significantly improves the efficiency of desirable (high current density, low capital cost) operating points. The limitations placed on air recirculation to prevent oxygen starvation in FC mode are also highlighted. As high air recirculation is found to be beneficial, more research is needed to study the degradation caused by oxygen starvation, and thereby determine more accurate upper limits for air recirculation.

Further, this work also finds that for a system with ideal heat integration, exergy destruction is minimised when ammonia is synthesised at a reaction (outlet) pressure of 170 bar, and the produced ammonia is separated by condensing it at 30 °C, without the need for refrigeration.

Exergy analysis of the optimised system design shows the major losses to be in the hot air exhaust from the FC mode, which could be reduced by the use of a bottoming power cycle utilising this heat. Other large exergy losses come from condensing the steam in FC mode, and evaporating water in EL mode. This suggests possible ideas for cross-mode integration (with thermal energy storage) between these two latent heat streams. It is also observed that internal cracking of ammonia can lead to large exergy losses, and analysing this further is a topic of ongoing research.

To conclude, this study shows ammonia to be a thermodynamically feasible option for energy storage when used in an rSOC-based system. This study adds to the growing body of research showing rSOC to be a valuable technology for supporting the growth of intermittent renewables, especially for balancing seasonal variations.

CRediT authorship contribution statement

Amogh Amladi: Methodology, Validation, Investigation, Visualization, Writing – original draft. **Vikrant Venkataraman:** Conceptualization, Writing – review & editing, Supervision. **Theo Woudstra:** Writing – review & editing, Supervision. **P.V. Aravind:** Conceptualization, Writing – review & editing, Supervision, Funding acquisition.

Declaration of competing interest

The authors declare that they have no known competing financial interests or personal relationships that could have appeared to influence the work reported in this paper.

Data availability

Data will be made available on request.

Acknowledgements

This work was a part of the BALANCE project, which received funding from the European Union's Horizon 2020 research and innovation programme under grant agreement No. 731224.

Appendix A. rSOC stack models

The rSOC stack model is adapted from the models of Hauck et al. [46]. Since Aspen Plus does not have a dedicated FC model, the model is developed as a simple thermochemical model, and the electrochemistry is programmed into the model through calculations made in an Aspen Plus calculator block. Schematics for the stack model in each mode are depicted in Figs. A.1(a) and A.1(b). The temperature is assumed to be uniform within the stack, and all the reactions are assumed to be isothermal at the temperature of the stack. The kinetics are assumed to be very fast due to the high stack temperatures.

The FC mode stack model is effectively built in three sections. The first section is the thermal management section, where the incoming fuel and air flows are heated up to the stack temperature by the stack body. This is followed by the cracking section, which contains an RSTOIC reactor block to emulate the complete internal cracking of ammonia by nickel in the fuel electrodes. Finally, the electrochemistry section consists of an ideal separator block which separates oxygen from the air stream in precisely the amount required to attain the required fuel utilisation, followed by an RSTOIC reactor block which oxidises the hydrogen produced from the ammonia. The electrolysis stack model is very similar, except the absence of a cracking section. In the electrochemical section, an RSTOIC reactor reduces a certain amount of steam into hydrogen to meet the desired steam utilisation value. The produced oxygen is the separated from the fuel side and mixed into the sweep air stream. The heat duty of all the RSTOIC reactors and the stream heaters is added to the stack body. In both modes, the airflow through the stack is controlled such that the net energy balance of the stack body is maintained. (It must be noted that the "stack body" shown in Figs. A.1(a) and A.1(b) is not an actual entity in the Aspen Plus model, but only a schematic visualisation of the energy balance calculations that are actually made in a calculator block in Aspen Plus.)

The electrochemical calculations and cell parameters are taken directly from the model of Hauck et al. [46], as was also done by Diaz-Rodriguez [14]. Those model were designed for fuel-electrode supported cells in CO_2-H_2O co-electrolysis systems. The carbon compounds were neglected for electrochemical calculations, since the carbon compounds were assumed to interact solely through water-gas shift and reverse water-gas shift reactions. Similarly, in the current work, nitrogen is considered electrochemically inert while ammonia is considered to be cracked only thermochemically, and hence the same electrochemical calculations for a hydrogen–steam system can be directly utilised. The reversible voltage averaged across the stack (U_{rev} [V]) is calculated using the current flowing through the stack (I [A]) and the actual change in Gibbs Energy flow ($\Delta\dot{G}$ [J]) between the inlets and outlets of the electrochemistry section of the stack model. This is shown in Eqs. (A.1a) and (A.1b), where the subscripts refer to streams in Figs. A.1(a) and A.1(b), respectively. The equations are written in such a way that the voltage is always positive.

$$U_{\mathrm{rev,FC}} = \frac{(\dot{G}_{\mathrm{FF3}} + \dot{G}_{\mathrm{FA2}}) - (\dot{G}_{\mathrm{FF4}} + \dot{G}_{\mathrm{FA3}})}{I} \tag{A.1a}$$

$$U_{\mathrm{rev,EL}} = \frac{(\dot{G}_{\mathrm{EF4}} + \dot{G}_{\mathrm{EA3}}) - (\dot{G}_{\mathrm{EF2}} + \dot{G}_{\mathrm{EA2}})}{I} \tag{A.1b}$$

The various electrochemical overpotentials are calculated individually. The values of various parameters used are shown in Table A.1,

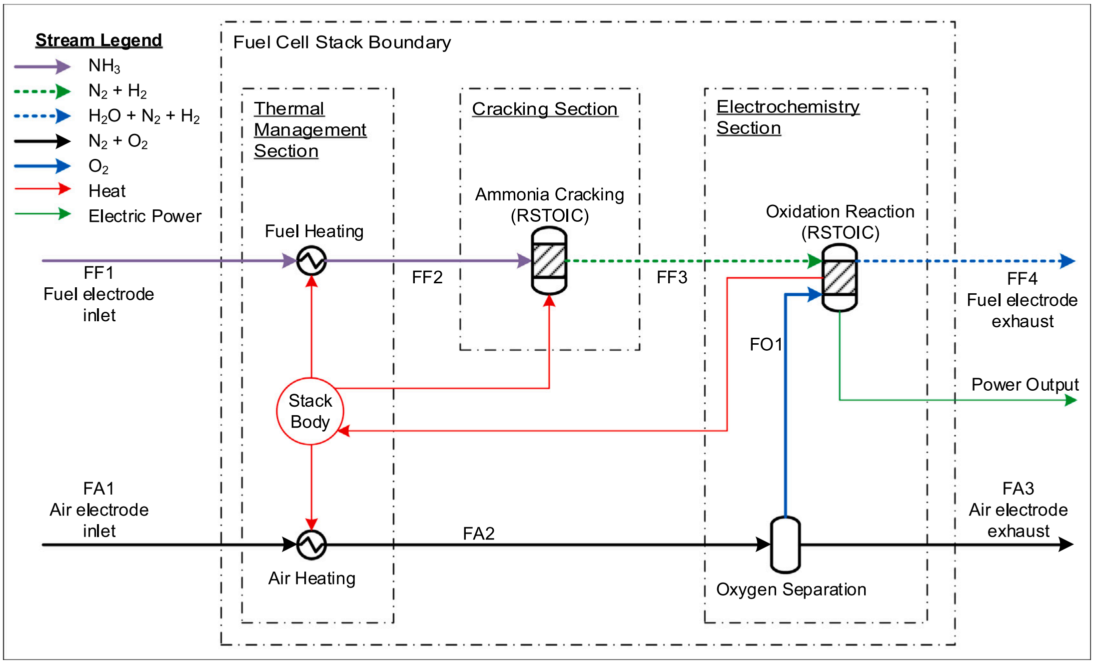

(a) Fuel cell mode

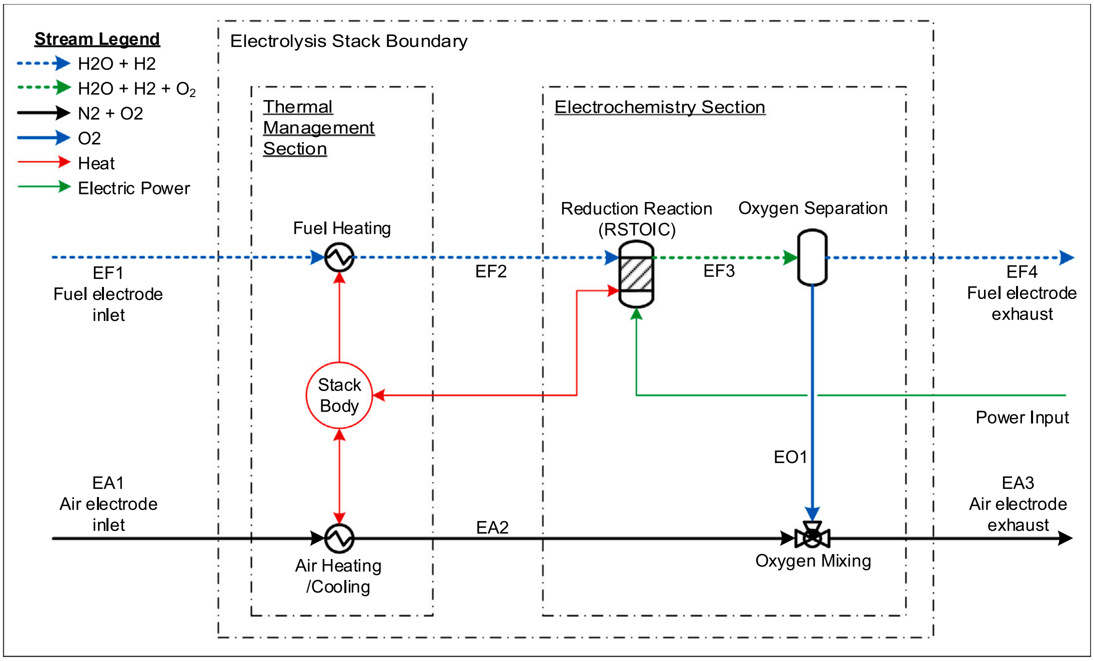

(b) Electrolyser mode

Fig. A.1. Schematic of the rSOC stack model.

Table A.1
Parameters for overpotential calculations [46].

Parameter	Symbol	Value	Unit
Number of electrons transferred — Fuel electrode	n_{FE}	2	$mol_{electron}/mol_{reactant}$
Symmetry factor — Fuel electrode	α_{FE}	0.5	–
Pre-exponential factor — Fuel electrode	γ_{FE}	1.34×10^{10}	$A\,m^{-2}$
Activation energy — Fuel electrode	$E_{act,FE}$	1.00×10^{5}	$J\,mol^{-1}$
Number of electrons transferred — Air electrode	n_{AE}	4	$mol_{electron}/mol_{reactant}$
Symmetry factor — Air electrode	α_{AE}	0.5	–
Pre-exponential factor — Air electrode	γ_{AE}	2.05×10^{9}	$A\,m^{-2}$
Activation energy — Air electrode	$E_{act,AE}$	1.20×10^{5}	$J\,mol^{-1}$
Electrolyte thickness	δ_{el}	1.25×10^{-5}	m
Pre-exponential factor — Electrolyte conductivity	$E_{act,el}$	3.33×10^{4}	$\Omega^{-1}\,m^{-1}$
Activation energy — Electrolyte conductivity	$E_{act,el}$	85 634	$J\,mol^{-1}$
Electronic area-specific Ohmic resistance	r_{const}	5.70×10^{-6}	$\Omega\,m^{2}$
Diffusion volume — Hydrogen	V_{d,H_2}	6.12	–
Diffusion volume — Water	V_{d,H_2O}	13.10	–
Diffusion volume — Oxygen	V_{d,O_2}	16.30	–
Diffusion volume — Nitrogen	V_{d,N_2}	18.50	–
Molecular mass — Hydrogen	M_{d,H_2}	2.02	$g\,mol^{-1}$
Molecular mass — Water	M_{d,H_2O}	18.02	$g\,mol^{-1}$
Molecular mass — Oxygen	M_{d,O_2}	32.00	$g\,mol^{-1}$
Molecular mass — Nitrogen	M_{d,N_2}	28.01	$g\,mol^{-1}$
Porosity of electrodes	ϵ	0.30	–
Tortuosity of electrodes	τ	5.00	–
Mean diameter of electrode pores	d_p	2.00×10^{-6}	m
Fuel Electrode Thickness (fitted)	δ_{FE}	3.20×10^{-5}	m
Air Electrode Thickness	δ_{AE}	1.75×10^{-5}	m

along with their symbols and units. Please refer to the original sources [14,46,69] for more details of the overpotential calculations.

The activation overpotential represents the activation energy of the reaction. The activation overpotential at electrode i ($\Delta U_{act,i}$ [V]) is calculated using the hyperbolic sine approximation to the Butler–Volmer equation, shown in Eq. (A.2). $j_{0,i}$ [$A\,m^{-2}$] is the exchange current density, calculated with an Arrhenius-type relation shown in Eq. (A.3), taken from Buttler et al. [33].

$$\Delta U_{act,i} = \frac{RT}{n_i F \alpha_i} \sinh^{-1}\left(\frac{j}{2 j_{0,i}}\right) \tag{A.2}$$

$$j_{0,i} = \gamma_i \exp\left(\frac{-E_{act,i}}{RT}\right) \tag{A.3}$$

The Ohmic overpotential (ΔU_{ohm} [V]) represents the losses due to the resistance offered by the various cell components to the flow of charge (ions or electrons). The ionic resistance of the electrolyte is much larger and more sensitive to temperature than the electronic resistance of the other components. Therefore, the electronic resistance r_{const} [$\Omega\,m^2$] is taken to be constant. The Ohmic overpotential is calculated with Eq. (A.4). σ_{el} [$\Omega^{-1}\,m^{-1}$] is the conductivity of the electrolyte, also calculated using an Arrhenius-type relation shown in Eq. (A.5).

$$\Delta U_{ohm} = j\left(\frac{\delta_{el}}{\sigma_{el}} + r_{const}\right) \tag{A.4}$$

$$\sigma_{el} = \sigma_{0,el} \exp\left(\frac{-E_{act,el}}{RT}\right) \tag{A.5}$$

Concentration overpotential represents losses due to the slow diffusive mass transfer through the electrodes. Due to slow mass transfer, the reaction sites (TPB) see different species concentrations compared to the bulk flow. The difference in voltages due to concentration difference is represented as concentration overpotential $\Delta U_{conc,i,j}$ at electrode i in mode j, as seen in Eq. (A.6).

$$\Delta U_{conc,FE,FC} = \frac{RT}{2F} \ln\left(\frac{p_{H_2,bulk} \cdot p_{H_2O,TPB}}{p_{H_2,TPB} \cdot p_{H_2O,bulk}}\right) \tag{A.6a}$$

$$\Delta U_{conc,FE,EC} = \frac{RT}{2F} \ln\left(\frac{p_{H_2,TPB} \cdot p_{H_2O,bulk}}{p_{H_2,bulk} \cdot p_{H_2O,TPB}}\right) \tag{A.6b}$$

$$\Delta U_{conc,AE,FC} = \frac{RT}{2F} \ln\left(\frac{p^{0.5}_{O_2,bulk}}{p^{0.5}_{O_2,TPB}}\right) \tag{A.6c}$$

$$\Delta U_{conc,AE,EC} = \frac{RT}{2F} \ln\left(\frac{p^{0.5}_{O_2,TPB}}{p^{0.5}_{O_2,bulk}}\right) \tag{A.6d}$$

The species partial pressures at the TPB are calculated using equation Eq. (A.7). For these equations, current density j [$A\,m^{-2}$] is considered positive for FC mode and negative for EL mode. Hauck et al. [46] introduced a new modification to the model, which was validated with experimental data. It was noticed that the concentration overpotentials predicted by the original model were higher than observed values. This was theorised to be caused by the porous support layer in the fuel electrode supported cell. The model considers the entire fuel electrode to be of the same porosity as the active layer. In practice, the support layer has significantly higher porosity than the active layer, and causes smaller diffusion losses. Thus, Hauck et al. modified the thickness of the fuel electrode δ_{FE} [m] in the model to fit the concentration overpotentials to the experimental data. This fitted value is used in this work as well, shown in Table A.1.

$$p_{H_2,TPB} = p_{H_2,bulk} - \frac{RT\delta_{FE} j}{2F D_{eff,H_2}} \tag{A.7a}$$

$$p_{H_2O,TPB} = p_{H_2O,bulk} + \frac{RT\delta_{FE} j}{2F D_{eff,H_2O}} \tag{A.7b}$$

$$p_{O_2,TPB} = p_{O_2,bulk} - \frac{RT\delta_{AE} j}{4F D_{eff,O_2}} \tag{A.7c}$$

Table B.1
Parameters for validation.

Parameter	Value	Unit
Stack temperature	850	°C
Stack pressure	1	bar
Stack area	16	cm^2
Fuel inflow	0.01859	mol/min
Hydrogen mole fraction in fuel	0.5	–
Steam mole fraction in fuel	0.5	–
Oxygen mole fraction in oxidant	1	–

The effective diffusion coefficient $D_{\mathrm{eff},i}$ $[\mathrm{m^2\,s^{-1}}]$ for species i is assumed to depend on the Knudsen diffusion coefficient $D_{\mathrm{Kn},i}$ $[\mathrm{m^2\,s^{-1}}]$ and binary molecular diffusion coefficient D_{i-k} $[\mathrm{m^2\,s^{-1}}]$ for species i and k, as shown in Eq. (A.8). The Knudsen diffusion coefficient is calculated with Eq. (A.9), while the binary diffusion coefficient is calculated with the Fuller equation, Eq. (A.10).

$$D_{\mathrm{eff},i} = \frac{\epsilon}{\tau}\frac{D_{\mathrm{Kn},i}D_{i-k}}{D_{\mathrm{Kn},i} + D_{i-k}} \tag{A.8}$$

$$D_{\mathrm{Kn},i} = \frac{d_{\mathrm{p}}}{3}\sqrt{\frac{8RT}{\pi M_i}} \tag{A.9}$$

$$D_{i-k} = \frac{1.43\times10^{-7}\cdot T^{1.75}}{p\sqrt{\frac{2M_iM_k}{M_i+M_k}}\left(V_{\mathrm{d},i}^{1/3}+V_{\mathrm{d},k}^{1/3}\right)^2} \tag{A.10}$$

The actual cell voltages $U_{\mathrm{cell},i}$ [V] in mode i are calculated with Eq. (A.11).

$$\begin{aligned} U_{\mathrm{cell,FC}} &= U_{\mathrm{rev,FC}} - \Delta U_{\mathrm{act,FE}} - \Delta U_{\mathrm{act,AE}} - \Delta U_{\mathrm{ohm}} \\ &\quad - \Delta U_{\mathrm{conc,FE,FC}} - \Delta U_{\mathrm{conc,AE,FC}} \end{aligned} \tag{A.11a}$$

$$\begin{aligned} U_{\mathrm{cell,EL}} &= U_{\mathrm{rev,EL}} + \Delta U_{\mathrm{act,FE}} + \Delta U_{\mathrm{act,AE}} + \Delta U_{\mathrm{ohm}} \\ &\quad + \Delta U_{\mathrm{conc,FE,EL}} + \Delta U_{\mathrm{conc,AE,EL}} \end{aligned} \tag{A.11b}$$

Appendix B. rSOC model validation

The rSOC stack model described above was validated with the experimental data from literature [70], also used by Hauck et al. [46] for their model. The parameters used for the validation are shown in Table B.1.

The I-V curve (current–voltage curve) results from the validation are shown in Fig. B.1. Focusing on the current density region where this study operates (between 2500 A $\mathrm{m^{-2}}$ and 10 000 A $\mathrm{m^{-2}}$ in each mode), the RMS deviation from the experiments is 2.69% in FC mode, and 1.90% in EL mode. The maximum deviation is 3.65% in FC mode and 3.53% in EL mode.

Appendix C. Refrigeration cycle

In the optimisation of the ammonia synthesis loop parameters, the condensing temperature and the required refrigeration play a significant role. Therefore, it was seen to be necessary to consider the variation of refrigeration co-efficient of performance (COP) with temperature. This is estimated using a vapour compression cycle using ammonia as the refrigerant (not to be confused with ammonia used as the energy storage medium in this paper). The cycle along with the parameters used for it are shown in Fig. C.1(a). The discrete COP values extracted from this model are fitted into a 10th degree polynomial with a maximum error of around 2%. The fitting is shown in Fig. C.1(b). The fitted polynomial is described by Eq. (C.1), where T_{ref} [°C] is the temperature of ammonia separation. This polynomial is then used in the main model.

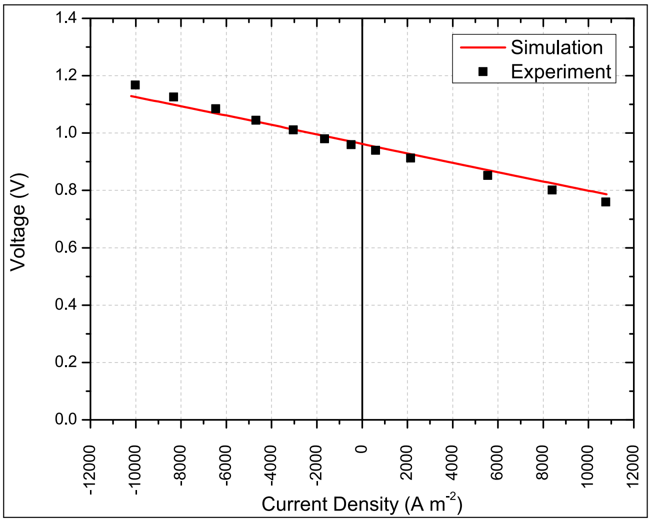

Fig. B.1. Validation results.

$$\begin{aligned} COP =& (1.64\times10^{-14})T_{\mathrm{ref}}^{10} + (1.31\times10^{-12})T_{\mathrm{ref}}^{9} \\ &+(6.26\times10^{-12})T_{\mathrm{ref}}^{8} - (1.55\times10^{-9})T_{\mathrm{ref}}^{7} \\ &-(1.81\times10^{-8})T_{\mathrm{ref}}^{6} + (8.66\times10^{-7})T_{\mathrm{ref}}^{5} \\ &+(1.47\times10^{-5})T_{\mathrm{ref}}^{4} - (2.65\times10^{-6})T_{\mathrm{ref}}^{3} \\ &+(2.98\times10^{-3})T_{\mathrm{ref}}^{2} + (1.65\times10^{-1})T_{\mathrm{ref}} + 4.39 \end{aligned} \tag{C.1}$$

Appendix D. Details on ammonia synthesis optimisation

D.1. Model

The flowsheet for the optimisation model is shown in Fig. D.1. It includes the synthesis loop elaborated in Section 2.3 and the multi-stage compressors from Section 2.4, with the modifications described further in this section.

The hydrogen produced in EL mode is immediately used for ammonia synthesis. The nitrogen-hydrogen mixture is produced in FC mode (from cracking and partial oxidation of ammonia) and stored in the interim. Therefore, the nitrogen-hydrogen compressor train has an additional cooler at the outlet to simulate heat loss during storage in the gas tank. This additional cooler (representing the gas tank) is not shown separately in Fig. D.1, but it is located at stream HB102. The inlet pressures of the hydrogen and nitrogen-hydrogen streams are based on the outlet pressure of their respective gas purification systems at various rSOC stack pressures.

The ammonia condensation is separated into cooling with ambient water, and refrigeration (if required, depending on the condensing temperature). A heat exchanger (named HEX in Fig. D.1) aids with refrigeration for the ammonia condenser (this is unnecessary when condenser temperature is 30 °C or more). The coefficient of performance for refrigeration is calculated with a vapour compression cycle, elaborated in Appendix C.

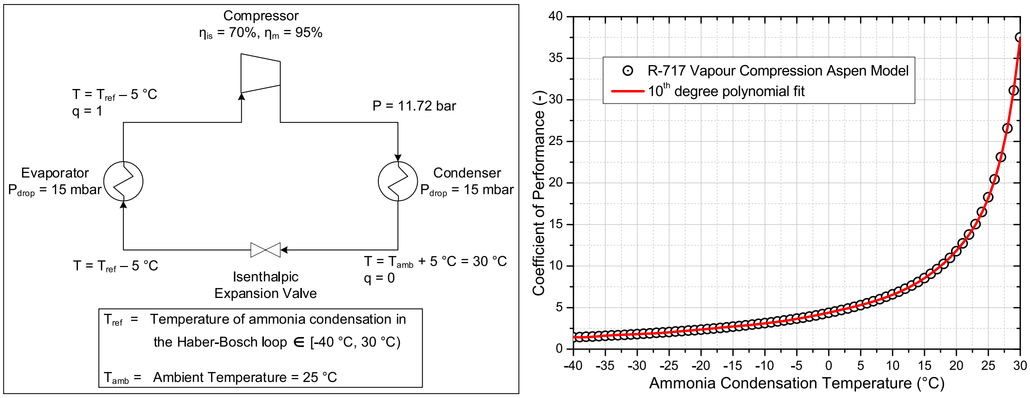

(a) Flowsheet of refrigeration cycle

(b) Co-efficient of performance results and polynomial fit

Fig. C.1. Refrigeration cycle for co-efficient of performance calculation.

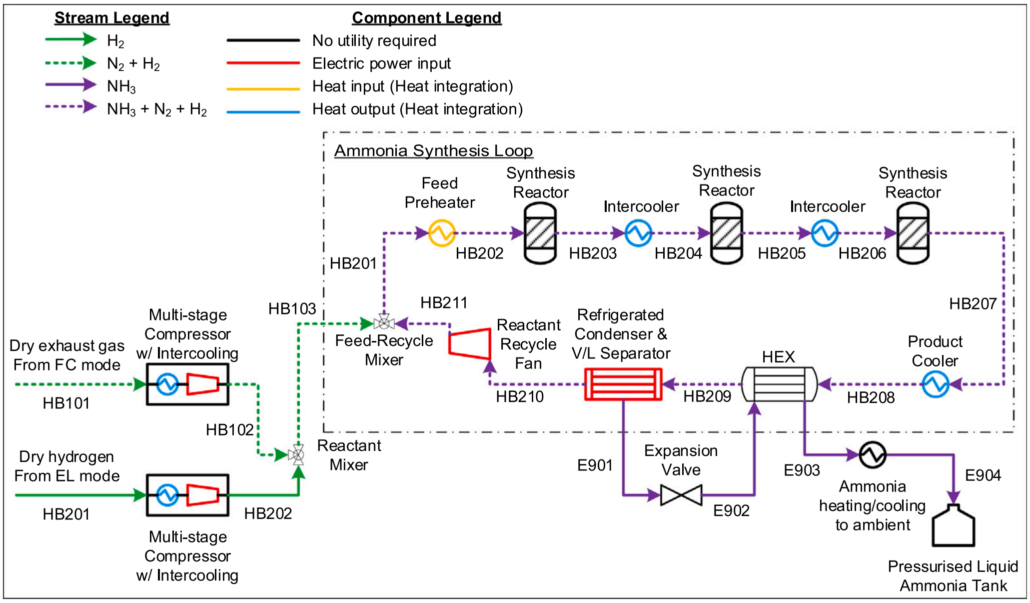

Fig. D.1. Flowsheet of the synthesis loop optimisation model.

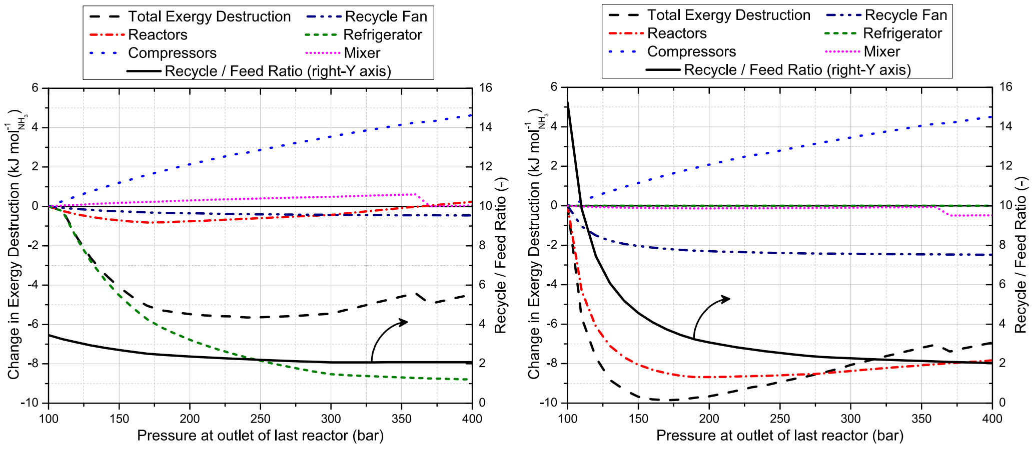

(a) Ammonia condensation at −30 °C

(b) Ammonia condensation at 30 °C

Fig. D.2. Effect of synthesis reaction pressure. Reversible solid oxide cell (rSOC) pressure for this example: 5 bar.

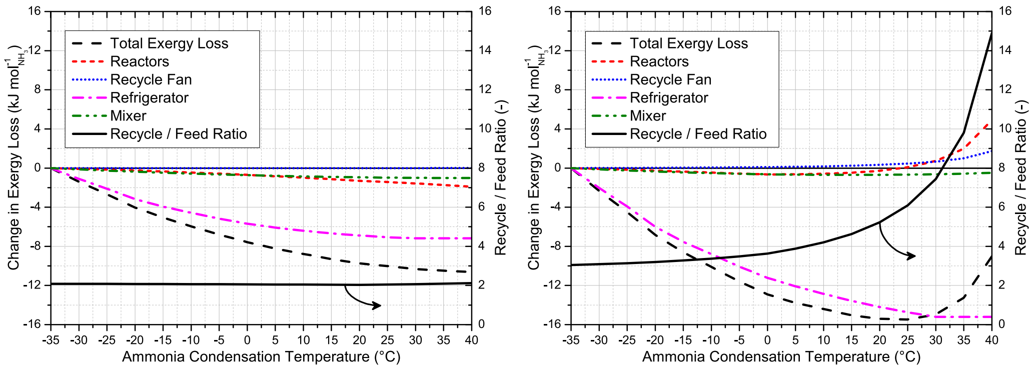

(a) Pressure at outlet of last reactor: 380 bar (b) Pressure at outlet of last reactor: 120 bar

Fig. D.3. Effect of ammonia condensation temperature. rSOC stack pressure for this example: 5 bar.

Table E.1
Stream table for fuel cell mode. Stream labels are from Fig. 1. Flow rates are per mole of NH_3 in stream F101. Stack operating point: 2500 A m^{-2}, 700 °C, 10 bar.

Stream	Temp.	Pres.	Molar	Flow rate	Mole fractions				
label	°C	bar	vap. frac.	mol/mol$_{NH_3}$	NH_3	N_2	H_2	H_2O	O_2
F101	25.000	11.000	0.00	1.000	1.000	–	–	–	–
F102	24.957	10.030	0.00	1.000	1.000	–	–	–	–
F103	24.957	10.030	0.00	1.000	1.000	–	–	–	–
F103–1	332.502	10.030	1.00	1.000	1.000	–	–	–	–
F103–2	600.000	10.030	1.00	1.000	1.000	–	–	–	–
F104	600.000	10.015	1.00	1.000	1.000	–	–	–	–
F201	700.000	10.000	1.00	2.000	–	0.250	0.150	0.600	–
F201–1	700.000	10.000	1.00	1.029	–	0.250	0.150	0.600	–
F201–2	337.502	10.000	1.00	1.029	–	0.250	0.150	0.600	–
F201–3	700.000	10.000	1.00	0.971	–	0.250	0.150	0.600	–
F201–4	337.502	10.000	1.00	0.971	–	0.250	0.150	0.600	–
F201–5	337.502	10.000	1.00	2.000	–	0.250	0.150	0.600	–
F201–6	148.683	10.000	0.74	2.000	–	0.250	0.150	0.600	–
F201–7	30.000	9.985	0.40	2.000	–	0.250	0.150	0.600	–
F202	30.000	9.985	1.00	0.803	–	0.623	0.374	0.003	–
F301	30.000	8.987	1.00	0.800	–	0.625	0.375	–	–
F302	25.000	185.045	1.00	0.800	–	0.625	0.375	–	–
F401	30.000	9.985	0.00	1.197	–	–	–	1.000	–
F402	30.194	1.028	0.00	1.197	–	–	–	1.000	–
F403	180.478	8.987	1.00	0.003	–	–	–	1.000	–
F404	167.904	1.028	1.00	0.003	–	–	–	1.000	–
F405	31.537	1.028	0.00	1.200	–	–	–	1.000	–
F406	25.000	1.013	0.00	1.200	–	–	–	1.000	–
F501	25.000	1.013	1.00	3.397	–	0.790	–	–	0.210
F502	332.502	10.030	1.00	3.397	–	0.790	–	–	0.210
F502–1	332.502	10.030	1.00	3.397	–	0.790	–	–	0.210
F502–2	451.789	10.030	1.00	3.397	–	0.790	–	–	0.210
F503	478.823	10.015	1.00	3.397	–	0.790	–	–	0.210
F504	600.000	10.015	1.00	7.455	–	0.882	–	–	0.118
F601	700.000	10.000	1.00	6.855	–	0.959	–	–	0.041
F602	700.000	10.000	1.00	2.797	–	0.959	–	–	0.041
F603	290.878	1.028	1.00	2.797	–	0.959	–	–	0.041
F604	290.878	1.013	1.00	2.797	–	0.959	–	–	0.041
F605	700.000	10.000	1.00	4.058	–	0.959	–	–	0.041
F606	700.437	10.015	1.00	4.058	–	0.959	–	–	0.041

The heat exchanger HEX is implemented in the model. All other heaters and coolers are assumed to be perfectly integrated, although the integration is not shown. This means, exergy of the heat extracted from coolers and the heat given to the heaters is simply tallied, and any remaining exergy of heat is assumed to be integrated outside the loop (i.e. in the rest of the rSOC system). This is a reasonable simplification, since the synthesis reaction produces more heat than required for the feed preheating, and the excess heat is indeed used in steam generation for electrolysis.

D.2. Effect of ammonia synthesis reaction pressure

The effect of reaction pressure on system exergy destruction depends on the condensation temperature. At low condensation temperatures, ammonia separation is very effective. Therefore, the ammonia content in the recycle and first reactor inlet streams is low. Therefore, this inlet mixture is far away from equilibrium, and the reactors can have a high reactant conversion. Due to high conversion and effective separation, recycle flow rates are small (only 2–3 times the fresh feed flow), as seen in Fig. D.2(a). Thanks to this, the recycle fan does not have to do a lot of work, and its exergy destruction is small. But the low condensation temperature requires the refrigerator to consume a lot of electricity and its exergy destruction is rather high. If the reaction pressure is increased, equilibrium favours the product and reactant conversion in the reactors increases further. Higher conversion makes the recycle flow smaller, which reduces the flow in the entire loop. This reduces the refrigerator power and its exergy destruction significantly. Meanwhile, higher reaction pressure means that the feed gases from the rSOC have to be compressed by a higher ratio. Therefore, the power and exergy destruction of the feed compressors increases with reaction pressure. Both these effects are prominently visible in Fig. D.2(a). Because of the opposing effects on the compressors and refrigerator mentioned above, the optimum pressure lies at an intermediate value. This is somewhere between 220 bar and 270 bar, for low condenser temperatures.

At high condensation temperatures, less ammonia is separated. Therefore, the ammonia content at the first reactor inlet remains high and the reactant conversion in the reactors is low. This leads to very high flow rates in recycle stream and the entire loop, for the same rate of ammonia production. At low reaction pressure, the equilibrium favours the reactant, further reducing conversion and exacerbating the problem. In this situation, the recycle flow can be as high as 15 times the fresh feed flow, as seen in Fig. D.2(b). Because this situation is so highly unfavourable, even a small increase in reaction pressure significantly relieves the situation, and the recycle flow rate reduces sharply. At higher pressures, the recycle flow rate reduces to similar values as in the low condensation temperature case.

At high condensation temperatures, refrigeration is low or absent, therefore its exergy destruction is negligible. The feed compressors are unaffected by condenser temperatures, and their exergy destruction increases with rising reaction pressure just like in the previous case. The high recycle rate at low pressures leads to high power consumption and exergy destruction for the recycle fan. As the recycle rate reduces, so does the exergy destruction in the fan. The exergy destruction in the reactors need a closer look.

Since the ammonia production rate from the synthesis loop is constant, the actual heat produced in the reactors is approximately independent of reaction pressure. However, when the recycle rate is large, this heat leads to a much lower temperature rise in the reactors. Since the same amount of reaction heat leads to a lower temperature of the product mixture, this means that the exergy destruction in the reactors is high when the recycle rate is high. Further, high flow rates also imply higher exergy destruction associated with the assumed pressure drop in the reactors (5 bar per stage). When the recycle rate drops sharply, this destruction in the reactors also reduces sharply, as seen in Fig. D.2(b). However, if the pressure is increased further and the recycle rate stabilises, the exergy destruction in the reactors increases slowly. Since increasing pressure moves the equilibrium towards the product, the inlet mixture gets further away from equilibrium. Therefore the reaction has a larger driving force, which implies greater irreversibility. This appears to be the cause of increasing exergy destruction.

Once again, because of the opposing effects of reaction pressure on exergy destruction in the compressors and reactors as explained above, the optimum pressure is at an intermediate value. However, in this case, the optimum pressure is relatively much lower, between 150 bar and 180 bar. This is because of the drastic change in exergy destruction in the reactor at low pressure due to the extremely high recycle rate variation, as explained above.

In both cases of Fig. D.2, one may notice a discontinuity in the total and mixer exergy loss curves at 360 bar. That is because at that point, the number of stages in the hydrogen compressor is increased from 5 to 6 (due to reaching the maximum stage-outlet temperature of 250 °C). This leads to a lower outlet temperature at the last stage, and thus smaller temperature difference between the fresh feed and recycle stream being mixed, and therefore lower mixing exergy losses. The impact on the losses in the compressors is relatively very small. A similar discontinuity does not exist for the nitrogen compressor (which is changed from 3 stages to 4 stages at 260 bar in this example), since that one has a cooler at the outlet, as mentioned in Appendix D.1.

D.3. Effect of ammonia condensation temperature

The effect of condensation temperature and reaction pressure on the recycle flow rate has already been explained in Appendix D.2, and will not be repeated here.

In general, condensation temperatures above ambient are found to be optimal. The largest benefit of increasing the condensation temperature is the reduction of refrigeration losses. As a higher temperature is used, the need for refrigeration reduces, and is eventually zero at 30 °C and beyond (not at the environment temperature 25 °C, because of a minimum 5 °C difference assumed for heat exchange).

The losses in the ammonia reactor generally decrease with a rise in condenser temperature. This is because as the ammonia separation gets less effective and ammonia concentration among the reactants increases, the driving force (and irreversibility) of the reaction decreases as mentioned in Appendix D.2. At high synthesis pressure, since the recycle rate is relatively stable, the recycle fan losses are constant, and the decline in reactor losses continues, as seen in Fig. D.3(a). Therefore, all the effects work in the same direction, leading to 40 °C (the highest temperature in this analysis) being the optimum condenser temperature.

However, at low reaction pressures, using high condenser temperatures leads to extremely high recycle rates, as discussed before. In this case, the reactor losses start to increase sharply due to exergy destruction from the transfer of reaction heat to the large flow of recycled reactants, and because of greater flow rates undergoing a pressure drop. The recycle fan losses also start mounting, as seen in Fig. D.3(b). Thus, there are opposing effects of raising the condenser temperature at low reaction pressures. Therefore, the optimum condenser temperature at low reaction pressures is not at the extremes, but lies between 25 °C and 35 °C.

Appendix E. Stream tables for optimum operating point

See Tables E.1 and E.2.

Table E.2
Stream table for electrolyser mode. Stream labels are from Fig. 2. Flow rates are per mole of NH_3 in stream E903. Stack operating point: 2500 A m^{-2}, 700 °C, 10 bar.

Stream	Temp.	Pres.	Molar	Flow rate	Mole fractions				
label	°C	bar	vap. frac.	mol/mol$_{NH_3}$	NH_3	N_2	H_2	H_2O	O_2
E101	25.000	1.013	0.00	1.463	–	–	–	1.000	–
E102	25.095	10.030	0.00	1.463	–	–	–	1.000	–
E102	25.095	10.030	0.00	1.463	–	–	–	1.000	–
E102–1	146.822	10.030	0.00	1.463	–	–	–	1.000	–
E102–2	180.073	10.030	0.09	1.463	–	–	–	1.000	–
E102–3	180.073	10.030	0.20	1.463	–	–	–	1.000	–
E102–4	180.073	10.030	0.49	1.463	–	–	–	1.000	–
E102–5	180.073	10.030	0.97	1.463	–	–	–	1.000	–
E102–6	194.046	10.030	1.00	1.463	–	–	–	1.000	–
E102–7	589.262	10.030	1.00	1.463	–	–	–	1.000	–
E103	589.262	10.015	1.00	1.463	–	–	–	1.000	–
E104	600.000	10.015	1.00	1.667	–	–	0.100	0.900	–
E201	700.000	10.000	1.00	1.667	–	–	0.820	0.180	–
E202	700.000	10.000	1.00	1.464	–	–	0.820	0.180	–
E202–1	216.855	10.000	1.00	1.464	–	–	0.820	0.180	–
E202–2	77.990	10.000	0.85	1.464	–	–	0.820	0.180	–
E202–3	30.000	9.985	0.82	1.464	–	–	0.820	0.180	–
E203	30.000	9.985	1.00	1.204	–	–	0.997	0.003	–
E204	700.000	10.000	1.00	0.203	–	–	0.820	0.180	–
E205	700.443	10.015	1.00	0.203	–	–	0.820	0.180	–
E301	30.000	0.998	1.00	1.200	–	–	1.000	–	–
E302	242.638	185.045	1.00	1.200	–	–	1.000	–	–
E401	30.000	9.985	0.00	0.260	–	–	–	1.000	–
E402	30.194	1.028	0.00	0.260	–	–	–	1.000	–
E403	30.000	9.970	0.00	0.004	–	–	–	1.000	–
E404	30.193	1.028	0.00	0.004	–	–	–	1.000	–
E405	30.194	1.028	0.00	0.264	–	–	–	1.000	–
E406	25.000	1.013	0.00	0.264	–	–	–	1.000	–
E501	–	–	–	–	–	–	–	–	–
E502	–	–	–	–	–	–	–	–	–
E503	–	–	–	–	–	–	–	–	–
E504	700.821	10.030	1.00	10.591	–	–	–	–	1.000
E505	800.000	10.015	1.00	10.591	–	–	–	–	1.000
E601	700.000	10.000	1.00	11.191	–	–	–	–	1.000
E602	700.000	10.000	1.00	0.600	–	–	–	–	1.000
E603	310.842	1.028	1.00	0.600	–	–	–	–	1.000
E603–1	310.842	1.028	1.00	0.600	–	–	–	–	1.000
E604	185.073	1.013	1.00	0.600	–	–	–	–	1.000
E605	700.000	10.000	1.00	10.591	–	–	–	–	1.000
E606	700.821	10.030	1.00	10.591	–	–	–	–	1.000
E701	25.000	185.045	1.00	0.800	–	0.625	0.375	–	–
E702	150.408	185.045	1.00	2.000	–	0.250	0.750	–	–
E801	60.365	185.045	1.00	9.477	0.087	0.228	0.685	–	–
E801–1	400.000	185.045	1.00	9.477	0.087	0.228	0.685	–	–
E802	400.000	185.030	1.00	9.477	0.087	0.228	0.685	–	–
E803	489.742	180.030	1.00	8.980	0.147	0.213	0.640	–	–
E803–1	400.000	180.030	1.00	8.980	0.147	0.213	0.640	–	–
E804	400.000	180.015	1.00	8.980	0.147	0.213	0.640	–	–
E805	456.285	175.015	1.00	8.673	0.188	0.203	0.609	–	–
E805–1	400.000	175.015	1.00	8.673	0.188	0.203	0.609	–	–
E806	400.000	175.000	1.00	8.673	0.188	0.203	0.609	–	–
E807	436.410	170.000	1.00	8.477	0.215	0.196	0.589	–	–
E807–1	417.100	170.000	1.00	8.477	0.215	0.196	0.589	–	–
E807–2	65.523	170.000	1.00	8.477	0.215	0.196	0.589	–	–
E807–3	30.000	169.985	0.88	8.477	0.215	0.196	0.589	–	–
E808	30.000	169.985	1.00	7.477	0.110	0.223	0.667	–	–
E809	38.616	185.045	1.00	7.477	0.110	0.223	0.667	–	–
E901	30.000	169.985	0.00	1.000	1.000	–	–	–	–
E902	27.996	11.015	0.01	1.000	1.000	–	–	–	–
E903	25.000	11.000	0.00	1.000	1.000	–	–	–	–

Appendix F. Nomenclature

List of abbreviations

BoP	Balance of plant
COP	Coefficient of performance
EL	Electrolysis
FC	Fuel cell
HEX	Heat exchanger
RGIBBS	Gibbs Energy minimisation reactor (Aspen Plus)
RMS	Root mean square
rSOC	Reversible solid oxide cell
RSTOIC	Stoichiometric reactor (Aspen Plus)
RTE	Round-trip efficiency
SOC	Solid oxide cell
TPB	Triple phase boundary
TRL	Technology Readiness Level
TSA	Temperature-swing adsorption

List of symbols

α	Symmetry factor for activation overpotentials [–]
γ	Pre-exponential factor for exchange current density $[\mathrm{A\,m^{-2}}]$
δ	Thickness [m]
ϵ	Porosity [–]
η	Efficiency [–]
σ	Conductivity $[\Omega^{-1}\,\mathrm{m}^{-1}]$
σ_0	Pre-exponential factor for conductivity $[\Omega^{-1}\,\mathrm{m}^{-1}]$
τ	Tortuosity [–]
COP	Coefficient of performance
D	Diffusion coefficient $[\mathrm{m^2\,s^{-1}}]$
d	Diameter [m]
E	Energy $[\mathrm{J\,mol^{-1}}]$
$\dot{E}x$	Exergy flow [W or normalised to $\mathrm{kJ/mol_{NH_3}}$]
F	Faraday Constant $[\mathrm{C\,mol^{-1}}]$
$\dot{G}$	Gibbs energy flow [W]
I	Electric current [A]
j	Current density $[\mathrm{A\,m^{-2}}]$
j_0	Exchange current density $[\mathrm{A\,m^{-2}}]$
M	Molecular mass $[\mathrm{g\,mol^{-1}}]$
n	Number of electrons transferred [–]
P	Electrical power [W or normalised to $\mathrm{kJ/mol_{NH_3}}$]
p	(Partial) pressure [bar or Pa]
R	Universal Gas Constant $[\mathrm{J\,mol^{-1}\,K^{-1}}]$
r_{const}	(Area-specific) resistance of electron conductors $[\Omega\,\mathrm{m}^2]$
T	Temperature [°C or K]
U	Voltage [V]
ΔU	Overpotential [V]
V	Diffusion volume $[\mathrm{m^3}]$

List of subscripts

act	Activation
AE	Air electrode
bulk	bulk flow in electrode channels
conc	Concentration
eff	Effective
EL	Electrolysis mode
el	Electrolyte
ex	Exergy
FC	Fuel cell mode
FE	Fuel electrode
i/k	Counter variables (to count electrodes, or gaseous compounds)
$i-k$	Binary (diffusion coefficient)
in	Input
Kn	Knudsen
net	Net (as opposed to gross)
ohm	Ohmic
out	Output
p	Pores
ref	Reference
rev	Reversible/Ideal
RT	Round-trip
TPB	Triple phase boundary

References

[1] IEA. Renewables 2019. Paris: IEA; 2019, URL https://www.iea.org/reports/renewables-2019. [Accessed 26 August 2020].

[2] Schermeyer Hans, Vergara Claudio, Fichtner Wolf. Renewable energy curtailment: A case study on today's and tomorrow's congestion management. Energy Policy 2018;112:427–36. http://dx.doi.org/10.1016/j.enpol.2017.10.037.

[3] Venkataraman Vikrant, Pérez-Fortes Mar, Wang Ligang, Hajimolana Yashar S, Boigues-Muñoz Carlos, Agostini Alessandro, et al. Reversible solid oxide systems for energy and chemical applications – Review & perspectives. J Energy Storage 2019;24:100782. http://dx.doi.org/10.1016/j.est.2019.100782.

[4] Glenk Gunther, Reichelstein Stefan. Reversible Power-to-Gas systems for energy conversion and storage. Nature Commun 2022;13(2010). http://dx.doi.org/10.1038/s41467-022-29520-0.

[5] Botta Giulia, Patel Hrishikesh C, Sebastiani Francesco, Aravind PV. Thermodynamic and exergy analysis of reversible solid oxide cell systems. ECS Trans 2015;68(1):3265–77. http://dx.doi.org/10.1149/06801.3265ecst.

[6] Di Giorgio Paolo, Desideri Umberto. Potential of reversible solid oxide cells as electricity storage system. Energies 2016;9(8). http://dx.doi.org/10.3390/en9080662.

[7] S. Santhanam, Heddrich MP, Riedel M, Friedrich KA. Theoretical and experimental study of Reversible Solid Oxide Cell (r-SOC) systems for energy storage. Energy 2017;141:202–14. http://dx.doi.org/10.1016/j.energy.2017.09.081.

[8] Santhanam Srikanth, Heddrich Marc, Riedel Marc, Friedrich K Andreas. Process design study of reversible solid oxide cell (r-SOC) system for coupling energy storage and hydrogen economy supply chain. ECS Trans 2017;78(1):2925–32.

[9] Frank Matthias, Deja Robert, Peters Roland, Blum Ludger, Stolten Detlef. Bypassing renewable variability with a reversible solid oxide cell plant. Appl Energy 2018;217:101–12. http://dx.doi.org/10.1016/j.apenergy.2018.02.115.

[10] Perna Alessandra, Minutillo Mariagiovanna, Jannelli Elio. Designing and analyzing an electric energy storage system based on reversible solid oxide cells. Energy Convers Manage 2018;159:381–95. http://dx.doi.org/10.1016/j.enconman.2017.12.082.

[11] Wang Ligang, Zhang Yumeng, Pérez-Fortes Mar, Aubin Philippe, Lin Tzu-En, Yang Yongping, et al. Reversible solid-oxide cell stack based power-to-x-to-power systems: Comparison of thermodynamic performance. Appl Energy 2020;275:115330. http://dx.doi.org/10.1016/j.apenergy.2020.115330.

[12] Mottaghizadeh Pegah, Santhanam Srikanth, Heddrich Marc P, Friedrich K Andreas, Rinaldi Fabio. Process modeling of a reversible solid oxide cell (r-SOC) energy storage system utilizing commercially available SOC reactor. Energy Convers Manage 2017;142:477–93. http://dx.doi.org/10.1016/j.enconman.2017.03.010.

[13] Reznicek Evan, Braun Robert J. Techno-economic and off-design analysis of stand-alone, distributed-scale reversible solid oxide cell energy storage systems. Energy Convers Manage 2018;175:263–77. http://dx.doi.org/10.1016/j.enconman.2018.08.087.

[14] Diaz Rodriguez Sebastian. Design and modeling of an energy storage system based on solid oxide reversible cells with syngas as fuel and co-electrolysis of CO_2 and H_2O. Delft University of Technology; 2018, URL http://resolver.tudelft.nl/uuid:4689ac2b-d4eb-4ace-a112-d63259c6f2ad.

[15] Jensen SH, Graves C, Mogensen M, Wendel C, Braun R, Hughes G, et al. Large-scale electricity storage utilizing reversible solid oxide cells combined with underground storage of CO_2 and CH_4. Energy Environ Sci 2015;8(8):2471–9. http://dx.doi.org/10.1039/C5EE01485A.

[16] Butera Giacomo, Jensen Søren Højgaard, Clausen Lasse Røngaard. A novel system for large-scale storage of electricity as synthetic natural gas using reversible pressurized solid oxide cells. Energy 2019;166:738–54. http://dx.doi.org/10.1016/j.energy.2018.10.079.

[17] Giannoulidis Sotiris, Venkataraman Vikrant, Woudstra Theo, Aravind PV. Methanol based Solid Oxide Reversible energy storage system – Does it make sense thermodynamically? Appl Energy 2020;278:115623. http://dx.doi.org/10.1016/j.apenergy.2020.115623.

[18] Wang Ganzhou, Mitsos Alexander, Marquardt Wolfgang. Conceptual design of ammonia-based energy storage system: System design and time-invariant performance. AIChE J 2017;63(5):1620–37. http://dx.doi.org/10.1002/aic.15660.

[19] Mukelabai Mulako Dean, Gillard Jonathon M, Patchigolla Kumar. A novel integration of a green power-to-ammonia to power system: Reversible solid oxide fuel cell for hydrogen and power production coupled with an ammonia synthesis unit. Int J Hydrogen Energy 2021;46(35):18546–56. http://dx.doi.org/10.1016/j.ijhydene.2021.02.218.

[20] Appl Max. Ammonia, 1. Introduction. In: Ullmann's encyclopedia of industrial chemistry. Wiley-VCH; 2011, http://dx.doi.org/10.1002/14356007.a02_143.pub3.

[21] Appl Max. Ammonia, 2. Production processes. In: Ullmann's encyclopedia of industrial chemistry. Wiley-VCH; 2011, http://dx.doi.org/10.1002/14356007.o02_o11.

[22] Cinti Giovanni, Discepoli Gabriele, Sisani Elena, Desideri Umberto. SOFC operating with ammonia: Stack test and system analysis. Int J Hydrogen Energy 2016;41(31):13583–90. http://dx.doi.org/10.1016/j.ijhydene.2016.06.070.

[23] Ma Qianli, Peng Ran Ran, Tian Longzhang, Meng Guangyao. Direct utilization of ammonia in intermediate-temperature solid oxide fuel cells. Electrochem Commun 2006;8(11):1791–5. http://dx.doi.org/10.1016/j.elecom.2006.08.012.

[24] Zhang Limin, Cong You, Yang Weishen, Lin Liwu. A direct ammonia tubular solid oxide fuel cell. Chinese J Catal 2007;28(9):749–51. http://dx.doi.org/10.1016/S1872-2067(07)60062-X.

[25] Dekker NJJ, Rietveld G. Highly efficient conversion of ammonia in electricity by solid oxide fuel cells. J Fuel Cell Sci Technol 2006;3(4):499–502. http://dx.doi.org/10.1115/1.2349536.

[26] Kazempoor P, Dorer V, Ommi F. Evaluation of hydrogen and methane-fuelled solid oxide fuel cell systems for residential applications: System design alternative and parameter study. Int J Hydrogen Energy 2009;34(20):8630–44. http://dx.doi.org/10.1016/j.ijhydene.2009.07.119.

[27] Liso Vincenzo, Olesen Anders Christian, Nielsen Mads Pagh, Kær Søren Knudsen. Performance comparison between partial oxidation and methane steam reforming processes for solid oxide fuel cell (SOFC) micro combined heat and power (CHP) system. Energy 2011;36(7):4216–26. http://dx.doi.org/10.1016/j.energy.2011.04.022.

[28] Woudstra Nico. Sustainable energy systems - limitations and challenges based on exergy analysis (Ph.D. thesis), Delft University of Technology; 2012, http://dx.doi.org/10.4233/uuid:112039e0-89ee-44fa-8d52-17eca3ec41f0.

[29] Gandiglio M, Lanzini A, Leone P, Santarelli M, Borchiellini R. Thermoeconomic analysis of large solid oxide fuel cell plants: Atmospheric vs. pressurized performance. Energy 2013;55:142–55. http://dx.doi.org/10.1016/j.energy.2013.03.059.

[30] Mehr AS, Mahmoudi SMS, Yari M, Chitsaz A. Thermodynamic and exergoeconomic analysis of biogas fed solid oxide fuel cell power plants emphasizing on anode and cathode recycling: A comparative study. Energy Convers Manage 2015;105:596–606. http://dx.doi.org/10.1016/j.enconman.2015.07.085.

[31] Botta G, Mor R, Patel H, Aravind PV. Thermodynamic evaluation of bi-directional solid oxide cell systems including year-round cumulative exergy analysis. Appl Energy 2018;226:1100–18. http://dx.doi.org/10.1016/j.apenergy.2018.05.061.

[32] Jeanmonod Guillaume, Wang Ligang, Diethelm Stefan, Maréchal François, Van Herle Jan. Trade-off designs of power-to-methane systems via solid-oxide electrolyzer and the application to biogas upgrading. Appl Energy 2019;247:572–81. http://dx.doi.org/10.1016/j.apenergy.2019.04.055.

[33] Buttler Alexander, Koltun Roman, Wolf Romano, Spliethoff Hartmut. A detailed techno-economic analysis of heat integration in high temperature electrolysis for efficient hydrogen production. Int J Hydrogen Energy 2015;40(1):38–50. http://dx.doi.org/10.1016/j.ijhydene.2014.10.048.

[34] Fu Qingxi, Mabilat Corentin, Zahid Mohsine, Brisse Annabelle, Gautier Ludmila. Syngas production via high-temperature steam/CO2 co-electrolysis: an economic assessment. Energy Environ Sci 2010;3:1382–97. http://dx.doi.org/10.1039/C0EE00092B.

[35] Sanz-Bermejo Javier, Muñoz-Antón Javier, Gonzalez-Aguilar José, Romero Manuel. Part load operation of a solid oxide electrolysis system for integration with renewable energy sources. Int J Hydrogen Energy 2015;40(26):8291–303. http://dx.doi.org/10.1016/j.ijhydene.2015.04.059.

[36] Saeedmanesh Alireza, Brouwer Jack. Dynamic modeling of a solid oxide electrolyzer system under two different thermal control strategies. In: Proceedings of 13th European SOFC & SOE forum 2018. 2018, p. A3129, URL https://www.efcf.com/efcf-library/proceedings-free/2019-1.

[37] Chen M, Sun X, Chatzichristodoulou C, Koch S, Hendriksen PV, Mogensen MB. Thermoneutral operation of solid oxide electrolysis cells in potentiostatic mode. ECS Trans 2017;78(1):3077–88.

[38] Petipas Floriane, Brisse Annabelle, Bouallou Chakib. Model-based behaviour of a high temperature electrolyser system operated at various loads. J Power Sources 2013;239:584–95. http://dx.doi.org/10.1016/j.jpowsour.2013.03.027.

[39] O'Brien JE, McKellar MG, Harvego EA, Stoots CM. High-temperature electrolysis for large-scale hydrogen and syngas production from nuclear energy – summary of system simulation and economic analyses. Int J Hydrogen Energy 2010;35:4808–19. http://dx.doi.org/10.1016/j.ijhydene.2009.09.009.

[40] Peters Ro, Frank M, Tiedemann W, Hoven I, Deja R, Kruse N, et al. Long-term experience with a 5/15kW-Class reversible solid oxide cell system. J Electrochem Soc 2021;168(1):014508. http://dx.doi.org/10.1149/1945-7111/abdc79.

[41] Giannoulidis Sotiris. A thermodynamic investigation of an electricity storage system based on reversible solid oxide cells with methanol as fuel and steam electrolysis. Delft University of Technology; 2018, URL http://resolver.tudelft.nl/uuid:9dce340b-e735-4307-9f96-49c093d96548.

[42] Ni Meng, Leung Dennis YC, Leung Michael KH. Electrochemical modeling of ammonia-fed solid oxide fuel cells based on proton conducting electrolyte. J Power Sources 2008;183(2):687–92. http://dx.doi.org/10.1016/j.jpowsour.2008.05.018.

[43] Fuerte Araceli, Valenzuela Rita Ximena, Escudero María José, Daza Loreto. Ammonia as efficient fuel for SOFC. J Power Sources 2009;192(1):170–4. http://dx.doi.org/10.1016/j.jpowsour.2008.11.037.

[44] Ni Meng. Thermo-electrochemical modeling of ammonia-fueled solid oxide fuel cells considering ammonia thermal decomposition in the anode. Int J Hydrogen Energy 2011;36(4):3153–66. http://dx.doi.org/10.1016/j.ijhydene.2010.11.100.

[45] Molouk Ahmed Fathi Salem, Okanishi Takeou, Muroyama Hiroki, Matsui Toshiaki, Eguchi Koichi. Electrochemical and catalytic behaviors of Ni-YSZ anode for the direct utilization of ammonia fuel in solid oxide fuel cells. J Electrochem Soc 2015;162(10):F1268–74. http://dx.doi.org/10.1149/2.1011510jes.

[46] Hauck Maximilian, Herrmann Stephan, Spliethoff Hartmut. Simulation of a reversible SOFC with Aspen Plus. Int J Hydrogen Energy 2017;42(15):10329–40. http://dx.doi.org/10.1016/j.ijhydene.2017.01.189.

[47] O'Brien JE. Thermodynamic considerations for thermal water splitting processes and high temperature electrolysis. In: Proceedings of the 2008 international mechanical engineering congress and exposition. 2008, http://dx.doi.org/10.1115/IMECE2008-68880.

[48] Khademi Mohammad Hasan, Sabbaghi Reyhaneh Sadat. Comparison between three types of ammonia synthesis reactor configurations in terms of cooling methods. Chem Eng Res Des 2017;128:306–17. http://dx.doi.org/10.1016/j.cherd.2017.10.021.

[49] Cheema Izzat Iqbal, Krewer Ulrike. Operating envelope of Haber–Bosch process design for power-to-ammonia. RSC Adv 2018;8(61):34926–36. http://dx.doi.org/10.1039/C8RA06821F.

[50] Kirova-Yordanova Zornitza. Exergy analysis of industrial ammonia synthesis. Energy 2004;29(12-15 SPEC. ISS):2373–84. http://dx.doi.org/10.1016/j.energy.2004.03.036.

[51] Tzimas Evangelos, Filiou C, Peteves Stathis Dimitris, Veyret Jean-Bernard. Hydrogen storage: State-of-the-art and future perspective. Petten, The Netherlands: European Commission Joint Research Centre; 2003, URL http://publications.jrc.ec.europa.eu/repository/handle/JRC26493. [Accessed 26 August 2020].

[52] Office of Energy Efficiency & Renewable Energy. Fuel cell technologies office: Multi-year research, development and demonstration plan. U.S. Department of Energy; 2012, URL https://www.energy.gov/sites/prod/files/2014/12/f19/fcto_myrdd_full_document.pdf. [Accessed 26 August 2020].

[53] Hartmann Niklas, Vöhringer O, Kruck C, Eltrop L. Simulation and analysis of different adiabatic Compressed Air Energy Storage plant configurations. Appl Energy 2012;93:541–8. http://dx.doi.org/10.1016/j.apenergy.2011.12.007, (1) Green Energy; (2) Special Section from papers presented at the 2nd International Energy 2030 Conference.

[54] UNEP. Energy efficiency guide for industry in Asia - Electrical energy equipment: Fans and blowers. 2006, URL http://www.energyefficiencyasia.org/docs/ee_modules/Chapter-Fans%20and%20Blowers.pdf. [Accessed 26 August 2020].

[55] Mohawk Innovative Technology Inc. High temperature anode recycle blowers for solid oxide fuel cell. 2018, URL https://www.netl.doe.gov/sites/default/files/2019-05/2019%20SOFC%20Proceedings/FE16-2019%20Fuel%20Cells%20Program%20Peer%20Eval%20Mtng%20Final.pdf. [Accessed 26 August 2021].

[56] CAP Co. Ltd. Anode gas recycle blower for SOFC. 2022, URL https://www.cap-co.jp/SOFCE.html. [Accessed 11 October 2022].

[57] Tomberg Marius, Heddrich Marc Philipp, Metten Matthias, Ansar Syed Asif, Friedrich Kaspar Andreas. Operation of a solid oxide fuel cell reactor with multiple stacks in a pressured system with fuel gas recirculation. Energy Technol 2022;10(4):2101075. http://dx.doi.org/10.1002/ente.202101075.

[58] Huang Yu, Merkel Tim C, Baker Richard W. Pressure ratio and its impact on membrane gas separation processes. J Membr Sci 2014;463:33–40. http://dx.doi.org/10.1016/j.memsci.2014.03.016.

[59] Tjaden B, Gandiglio M, Lanzini A, Santarelli M, Järvinen M. Small-scale biogas-SOFC plant: Technical analysis and assessment of different fuel reforming options. Energy Fuels 2014;28(6):4216–32. http://dx.doi.org/10.1021/ef500212j.

[60] Xiang JY, Calì M, Santarelli M. Calculation for physical and chemical exergy of flows in systems elaborating mixed-phase flows and a case study in an IRSOFC plant. Int J Energy Res 2004;28(2):101–15. http://dx.doi.org/10.1002/er.953.

[61] Morris David R, Szargut Jan. Standard chemical exergy of some elements and compounds on the planet earth. Energy 1986;11(8):733–55. http://dx.doi.org/10.1016/0360-5442(86)90013-7.

[62] Braun Robert J, Vincent Tyrone L, Zhu Huayang, Kee Robert J. Chapter 7 - analysis, optimization, and control of solid-oxide fuel cell systems. In: Sundmacher Kai, editor. Fuel cell engineering. Advances in chemical engineering, vol. 41, Academic Press; 2012, p. 383–446. http://dx.doi.org/10.1016/B978-0-12-386874-9.00011-7.

[63] Thambiraj Nelson, Suciu Crina, Waernhus Ivar, Vik Arild, Hoffmann Alex C. Effect of oxygen depletion to the cathode on the working of solid oxide fuel cells. ECS Trans 2017;78(1):875–87. http://dx.doi.org/10.1149/07801.0875ecst.

[64] Sohal Manohar S, Herring J Stephen. Oxygen handling and cooling options in high temperature electrolysis plants. Idaho National Lab; 2008, http://dx.doi.org/10.2172/936626.

[65] Reytier M, Di Iorio S, Chatroux A, Petitjean M, Cren J, De Saint Jean M, et al. Stack performances in high temperature steam electrolysis and co-electrolysis. Int J Hydrogen Energy 2015;40(35):11370–7. http://dx.doi.org/10.1016/j.ijhydene.2015.04.085.

[66] Liu Tong-Le, Wang Cheng, Hao Si-Jia, Fu Zhi-Qiang, Peppley Brant A, Mao Zhi-Ming, et al. Evaluation of polarization and hydrogen production efficiency of solid oxide electrolysis stack with $La_{0.6}Sr_{0.4}Co_{0.2}Fe_{0.8}O_3$-$\delta$-$Ce_{0.9}Gd_{0.1}O_{1.95}$ oxygen electrode. Int J Hydrogen Energy 2016;41(36):15970–8. http://dx.doi.org/10.1016/j.ijhydene.2016.04.243, Special Issue: 16th China Hydrogen Energy Conference (CHEC 2015), November 2015, Zhenjiang City, Jiangsu Province, China.

[67] Subotić Vanja, Futamura Shotaro, Harrington George F, Matsuda Junko, Natsukoshi Katsuya, Sasaki Kazunari. Towards understanding of oxygen electrode processes during solid oxide electrolysis operation to improve simultaneous fuel and oxygen generation. J Power Sources 2021;492:229600. http://dx.doi.org/10.1016/j.jpowsour.2021.229600.

[68] Smith Collin, Hill Alfred K, Torrente-Murciano Laura. Current and future role of Haber–Bosch ammonia in a carbon-free energy landscape. Energy Environ Sci 2020;13:331–44. http://dx.doi.org/10.1039/C9EE02873K.

[69] Amladi Amogh G. Process chain development of a ReSOC system with ammonia as fuel and steam electrolysis. Delft University of Technology; 2020, URL http://resolver.tudelft.nl/uuid:ae191dad-e925-481e-89e1-061d3271c921.

[70] Kazempoor P, Braun RJ. Model validation and performance analysis of regenerative solid oxide cells for energy storage applications: Reversible operation. Int J Hydrogen Energy 2014;39(11):5955–71. http://dx.doi.org/10.1016/j.ijhydene.2014.01.186.